น้ำหนุนในอ่าวไทยที่เกิดจากพายุไต้ฝุ่นลินดาในปี พ.ศ.2540 โดยใช้แบบจำลอง POM

นางสาวจิตราภรณ์ ฟักโสภา

วิทยานิพนธ์นี้เป็นส่วนหนึ่งของการศึกษาตามหลักสูตรปริญญาวิทยาศาสตรมหาบัณฑิต
สาขาวิชาวิทยาศาสตรมหาบัณฑิต ภาควิชาวิทยาศาสตร์ทางทะเล
คณะวิทยาศาสตร์ทางทะเล จุฬาลงกรณ์มหาวิทยาลัย
ปีการศึกษา 2546
ISBN 974-17-5240-7

STORM SURGE IN THE GULF OF THAILAND GENERATED BY TYPHOON LINDA IN 1997 USING PRINCETON OCEAN MODEL (POM)

Miss Jitraporn Phaksopa

A Thesis Submitted in Partial Fulfillment of the Requirements
for the Degree of Master of Science in Marine Science

Department of Marine Science
Faculty of Science
Chulalongkorn University

Academic Year 2003

ISBN 974-17-5240-7

Thesis Title	STORM SURGE IN THE GULF OF THAILAND GENERATED BY TYPHOON LINDA IN 1997 USING PRINCETON OCEAN MODEL (POM)
By	Miss Jitraporn Phaksopa
Field of Study	Marine Science
Thesis Advisor	Pramot Sojisuporn, Ph.D.

Accepted by the Faculty of Science, Chulalongkorn University in Partial Fulfillment of the Requirements for the Master's Degree

…….. Dean of Faculty of Science
(Professor Piamsak Menasveta, Ph.D.)

THESIS COMMITTEE

…….. Chairman
(Associate Absornsuda Siripong, M.S.)

…….. Thesis Advisor
(Pramot Sojisuporn, Ph.D.)

…….. Member
(Supichai Tangjaitrong, Ph.D.)

…….. Member
(Assistant Professor Somboon Pornpinatepong, Ph.D.)

จิตราภรณ์ ฟักโสภา : น้ำหนุนในอ่าวไทยที่เกิดจากพายุไต้ฝุ่นลินดาในปี พ.ศ.2540 โดยใช้แบบจำลอง POM (STORM SURGE IN THE GULF OF THAILAND GENERATED BY TYPHOON LINDA IN 1997 USING PRINCETON OCEAN MODEL (POM))
อ.ที่ปรึกษา: อ.ดร.ปราโมทย์ โศจิศุภร, 82 หน้า. ISBN 974-17-5240-7.

จำลองการไหลเวียนของน้ำเนื่องจากน้ำขึ้นน้ำลงในอ่าวไทยด้วยแบบจำลอง Princeton Ocean Model (POM) โดยใช้กริดขนาด 0.1° x 0.1° (11x11 ตารางกิโลเมตร) และใส่อิทธิพลของน้ำขึ้นน้ำลงที่ขอบเขตเปิดโดยใช้องค์ประกอบหลัก 8 ตัว คือ M_2, K_1, O_1, S_2, Q_1, P_1, K_2, N_2 ตรวจสอบความถูกต้องของแบบจำลองโดยเปรียบเทียบกับข้อมูลระดับน้ำจากสถานีวัดระดับน้ำในอ่าวไทย 23 สถานี พบว่าแบบจำลองสามารถจำลองระดับน้ำขึ้นน้ำลงได้ใกล้เคียงกับระดับน้ำจากสถานีวัด จากนั้นนำ POM ที่ได้ไปจำลองระดับน้ำขณะที่พายุไต้ฝุ่นลินดาพัดผ่านอ่าวไทยในเดือนพฤศจิกายน พ.ศ. 2540 ในการจำลองนี้ใส่อิทธิพลของน้ำขึ้นน้ำลงที่ขอบเขตเปิด ใส่ข้อมูลความกดอากาศ และข้อมูลลมทุก 12 ชั่วโมงจาก Navy Operational Global Atmosphere Prediction System (NOGAPS) ที่ผิวน้ำ พบว่า POM สามารถทำนายระดับน้ำในกรณีที่มีพายุหมุนเขตร้อนที่พัดเข้ามาในอ่าวไทยได้แต่ระดับน้ำขึ้นสูงสุดขณะเกิดน้ำหนุนที่ได้จากแบบจำลองมีค่าต่ำกว่าระดับน้ำจากสถานีวัดและคำนวณเวลาคลาดเคลื่อนประมาณ 1 ชั่วโมง เนื่องจากข้อมูลลมและความกดอากาศที่นำมาใช้มีค่าต่ำกว่าข้อมูลจริง นอกจากนี้ยังพบว่าข้อมูลลักษณะภูมิประเทศและความลึกน้ำจากฐานข้อมูล ETOPO5 ที่นำมาใช้มีความละเอียดต่ำจึงทำให้ค่าระดับน้ำที่คำนวณได้มีความคลาดเคลื่อน

ภาควิชา……วิทยาศาสตร์ทางทะเล…… ลายมือชื่อนิสิต.....……..
สาขาวิชา.....วิทยาศาสตร์ทางทะเล…… ลายมืออาจารย์ที่ปรึกษา.....……..
ปีการศึกษา....2546.....……..

4472235523 :MAJOR MARINE SCIENCE

KEYWORD: STORM SURGE / GULF OF THAILAND / PRINCETON OCEAN MODEL / TYPHOON LINDA

JITRAPORN PHAKSOPA: STORM SURGE IN THE GULF OF THAILAND GENERATED BY TYPHOON LINDA IN 1997 USING PRINCETON OCEAN MODEL (POM). THESIS ADVISOR : PRAMOT SOJISUPORN, Ph.D., pp.82 ISBN 974-17-5240-7.

Princeton Ocean Model (POM) was applied to simulate tidal circulation in the Gulf of Thailand. The model grid space was 0.1° x 0.1° (11x11 km^2). The model was forced by eight tidal components (M2, K1, O1, S2, Q1, P1, K2, and N2) at the open boundary. The model results were verified using tidal data from 23 tide gauges in the Gulf of Thailand. The results showed that the calculated values from POM corresponded well with the observed ones. Then, the model was used to simulate sea level fluctuation in response to typhoon Linda which entered the Gulf in November 1997. In addition to tidal forcing at the open boundary, 12-hours predicted atmospheric pressure and wind field from Navy Operational Global Atmosphere Prediction System (NOGAPS) were forced above the model surface. The model results showed that POM can simulate Linda's storm-surge even though the model underestimated the peak rise and sea level fluctuation was out of phase by approximately 1 hour sometimes. The reason for this might be that coarse grid, average atmospheric and wind fields were used in this study. In addition, the unreal of land-sea boundary and depth value from ETOPO5 might give rise to abnormal high sea level at some area in the model.

Department…. Marine Science …… Student's signature…….

Field of study…Marine Science …… Advisor's signature…….

Academic year…2003……

ACKNOWLEDGEMENTS

I would like to express my sincere gratitude to Dr. Pramot Sojisuporn, thesis advisor, for his encouragement and support that I had received throughout my study.

The support provided by the following organizations are appreciated, namely, Department and Promotion for Science and Technology talents Project of Thailand for granting the scholarship; the Hydrographic Department for data from tide gauge stations; the Department of Marine Science, Faculty of Science, Chulalongkorn University, for computer facilities.

Also, I am especially grateful to Dr. Sanit Piyawattanakorn for his help and encouragement and I would like to thank Pattama Singharuck for her advice about numerical model; Jariya Thitiwate for her help and friends at the Department of Marine Science for their helps and encouragements.

Lastly, I am indebted to my parents, brother for their understanding and continuing support.

CONTENTS

Page

LIST OF TABLES

LIST OF FIGURES

LIST OF FIGURES

CHAPTER 1

INTRODUCTION

Introduction

Storm surge, an abnormal high sea level phenomenon, is generated by very low pressure accompanied with very strong wind (tropical storm). Naturally, the water can flow freely in the open sea during the occurring of tropical storm, but not on land. Therefore, water is piled-up at the shore and spilled over lands. This causes serious hazards to coastal regions, such as flooding, coastal erosion, etc., and devastating the residential properties in those areas.

In Thailand, the occurring frequency of the tropical storm is about once in every two years and some can cause severe damage to lives and properties in the coastal area. For example, in 1962, typhoon Harriet hit Leam Talumpuk, Changwat Nakorn Srithammarat and caused severe damages to the area including more than 900 casualties. In 1989 typhoon Gay hit Changwat Chumporn causing serious disaster, such as destroying the agricultural lands (about 183,000 ha), killing over 400 people, and directly affecting 154,000 people. In 1997 typhoon Linda striked at Thupsake, Changwat Prachuapkirikhan, resulting in 30 people death, 102 people missing, and more than 400,000 Rai of agricultural land destroyed.

Thus, the warning system is needed for people who live in risking coastal areas. At present, there is no such warning system for coastal region in Thailand. The aim of this research is to examine how storm surge affect sea surface elevation and to apply a numerical model to predict the sea surface elevation disturbed by tropical storms in the Gulf of Thailand. In this study, Typhoon Linda was used because we have sufficient data not only to serve as inputs in the model, but also to verify the model results. The result from this study is useful in developing the warning system in the future.

Objective

To simulate the sea surface elevation during the storm surge occurrence using a hydrodynamical model

Scope of study

Numerical modeling (Princeton Ocean Model: POM) will be used to simulate the sea surface elevation and current in the Gulf of Thailand which were disturbed by typhoon Linda during the period of October 20, to November 9, 1997.

Prospective outcome

The couple tide and storm surge forecasting model for the Gulf of Thailand.

CHAPTER 2

LITERATURE REVIEWS

2.1 The characteristics of the Gulf of Thailand

The Gulf of Thailand is a semi-enclosed gulf located between Latitude 6° N to 13° N and Longitude 99° E to 105° E. The Gulf is bounded on the east by the coastline of Vietnam and the South China Sea, and the west by the coastlines of southern Thailand and Malaysia. The northern boundary of the Gulf is bordered by the coastline of Thailand. The Gulf connected to the South China Sea via southern entrance. Two sills restrict the flow at the entrance of the Gulf. The first sill runs from Kota Bharu to the Gulf center (northeast direction) for about 160 km, and the other one runs from Camau Peninsula of Vietnam to the southwestward for approximately 100 km. The water depth above the sills is around 25 km, while the depth at the main channel is around 70 m. The maximum depth at the center of The Gulf is about 80 m. The upper part of the Gulf is rather shallow with the mean depth of 15 m (Robinson, 1974).

The circulation in the Gulf of Thailand is complex because it is dominated by the combination of wind (wind-driven current), tide, density gradient, and the bathymetry of the Gulf (Oonpan, 2003). A large number of researches in this subject has been carried out by various methods such as numerical modeling (Yanagi and Takao, 1998; Oonpan, 2003), field observation (Robinson, 1974), and satellite data analysis (Morimoto *et al*, 2000). However, these studies could not provide the exact circulation pattern in the Gulf since there was no long-term observation data to verify the study results.

The major monsoons over the Gulf area are the northeast monsoon that prevails in November to February and the Southwest monsoon that prevails in May to September. Moreover, there are two transition periods between the opposing monsoon winds as depicted in Figure 2.1.

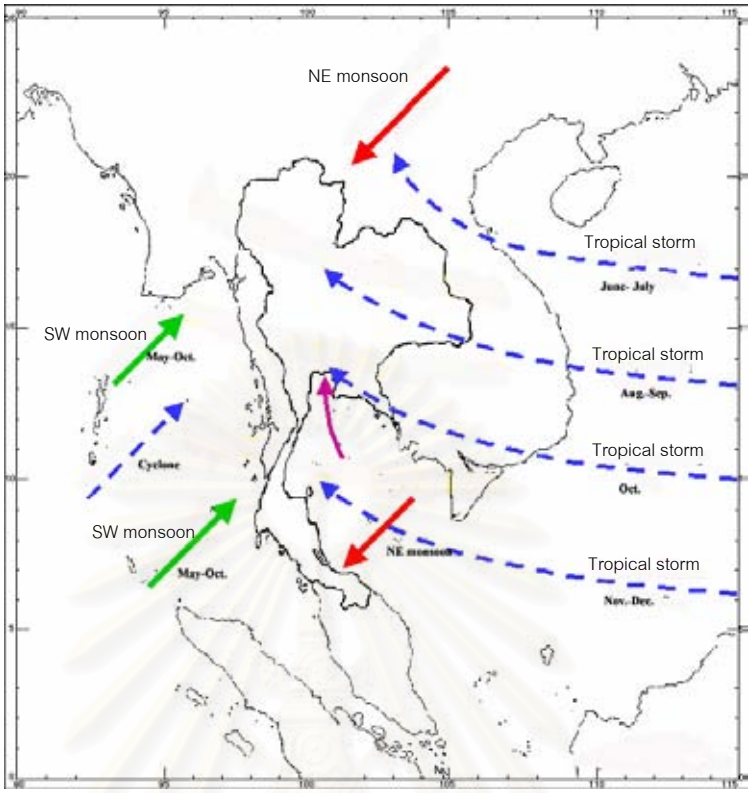

Figure 2.1 The prevailing wind of the Gulf of Thailand

(**from**:http://www.tmd.go.th/knowledge/image_know/season_03.jpg)

Every summer, southern Asia and especially India, is drenched by rain that comes from moist air masses that move in from the Indian Ocean to the south. These rains, and the air masses that bring them, are known as monsoons.

However, the term monsoon refers not only to the summer rains but to the entire cycle that consists of both summer moist onshore winds and rain from the south as well as the offshore dry winter winds that blow from the continent to the Indian Ocean.

In the summer, a high pressure area lies over the Indian Ocean while a low exists over the Asian continent. The air masses move from the high pressure over the ocean to the low over the continent, bringing moisture-laden air to south Asia.

During winter, the process is reversed and a low sits over the Indian Ocean while a high lies over the Tibetan plateau so air flows down the Himalaya and south to the ocean. The migration of trade winds and westerlies also contributes to the monsoons.

Tides in the Gulf of Thailand are the result of tidal waves propagation from the South China Sea, which are known as co-oscillation tides (Wyrtki, 1961 cited in Singharuck, 2002). The analysis of the tidal data from tide gauges revealed that the amplitudes of diurnal components are larger than the semidiurnal components (Johnston, 1998). Co-tidal chart from the numerical results (Singharuck, 2002) and satellite altimetry data (Yanagi *et al.*,1997) showed that the amphidromic system of the semi-diurnal components (M_2, S_2) rotated clockwise and their nodal axis aligned on NW-SE direction, while the amphidromic system of the diurnal components (K_1, O_1) rotated counter-clockwise and their nodal axis aligned on NE-SW direction. From the observation data, the upper Gulf of Thailand is dominated by mixed tide (semidiurnal dominate), while mixed tide (diurnal dominate) prevails in the further area from the inner Gulf. The diurnal tide is prevalent along the eastern and western sides of the Gulf. At the upper and southern part of Malay Peninsular, mixed diurnal-dominated tide and mixed semidiurnal-dominated tide prevail respectively (Johnston, 1998 cited in Siripong, 1985).

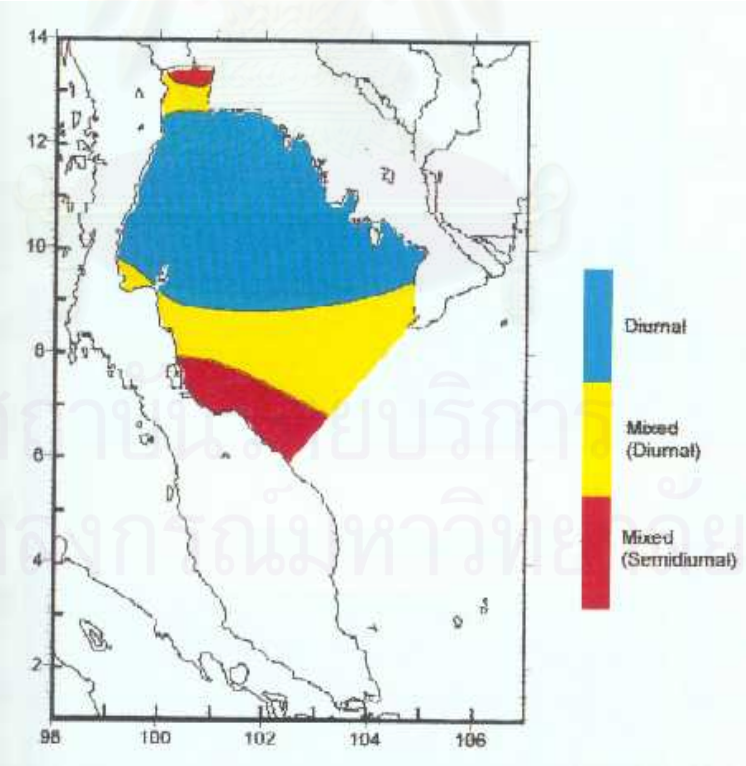

Figure 2.2 Tidal type in the Gulf of Thailand

(**from:** SEAPOL INTEGRATED STUDIES OF THE GULF OF THAILAND)

2.2 Storm surge

2.2.1 Characteristics of storm surge

Strom surge is an abnormal high sea level phenomenon caused by very low atmospheric pressure and very strong wind (storm). The storms form only over tropical oceans with surface temperature of 26°C or more (Smith, 1996) and need vorticity to give the low pressure system its initial rotation. As a result of the Coriolis force, the airflow converging on a low pressure is deflected to produce a favorable spiral. They hardly originate closer than 5°or 6° to the equator but occur most frequently between latitudes 10° and 20°. The direction of surface wind is a spiral shape which has the angle of 30° to the isobars, counter-clockwise in the northern hemisphere, and clockwise in the southern hemisphere (Humphreys, 1964).

There are two types of storm. The first one is tropical storms, which are generated in the sea, and are generally small and intense. They move from the point of origin in an unpredicted way until they meet the coast. Tropical storms are called variously in many locales as described below:

Name	Location
Cyclone	The Indian Ocean, Bay of Bengal
Typhoons	Japan
Hurricanes	The Caribbean, Gulf of Mexico, the Atlantic Ocean
Willi-willi	Australia

Storm's severities can be classified according to either the central pressure or the maximum wind speed at the storm's center.

Tropical depression	< 34 knots (63 km/hr.)
Tropical storm	34-64 knots (63-118 km/hr)
Typhoon	> 64 knots (118 km/hr)

The other storm is the extra tropical storm. They are slow moving and cover large area. So, they affect a wide area and take several days to die out (Pugh, 1987).

The factors that may cause sea level rise during the passage of a cyclonic storm are:

2.2.1.1 wind stress

The effect of wind on the sea level is given by (Pugh, 1987)

$$\frac{\partial \eta}{\partial x} = \frac{C_D \rho_a W^2}{g \rho D} \qquad (2.1)$$

The water depth (D) has inversely affected the sea surface elevation (η) , but the wind speed at the specific height (10m) directly affect on the sea surface elevation.

2.2.1.2 atmospheric pressure

A decrease in atmospheric pressure is accompanied by an increase in sea level called “inverted barometer effect” (Bowden, 1983)

$$\Delta \eta = \frac{-1}{g \rho} \Delta P_a \qquad (2.2)$$

According to the above equation, the pressure decrease for 1 mb corresponds to about 1 cm rise in sea level.

2.2.1.3 Wave set up from the storm wave

Wave setup occurs between the break-point and the beach, and is caused by the water from broken waves being pounded against the shore by incoming waves. It can be as much as 10-20% of the incident wave height.

2.2.1.4 Heavy rainfall

Heavy rainfall is always coincident with the storm. As a result, the water level in estuarine and lagoon rise due to freshwater runoff.

2.2.2 The impact of storm surge

Storm can cause severe disastrous effects on various coastal areas around the world. The Bay of Bengal in the Indian Ocean is seriously affected by the storm and disastrous flooding had occurred on a number of occasions. In 1970, surge caused by cyclone piled the water up to 7 m, claimed more than 300,000 lives. In the United States, Hurricane Hugo in September 1989, devastated 1.8 million hectares of timberland in 8 counties, and water damaged forest habitats (Chapman, 1994).

There were 5 severe storms (typhoons) that previously crossed over the Gulf of Thailand, namely typhoon “GAY” (November,1989), typhoon “BECKY” (August,1990), typhoon “FRED” (August,1991), typhoon “FOREST” (November,1992), typhoon “LINDA”(November,1997)(Lekphiphol,1998). Typhoon “GAY” caused more than 458 lives, affected 154,000 people, damaged 183,000 Ha of agricultural land and 20,000 livestock. In 1997 typhoon Linda striked at Thupsake, Changwat Prachupkirikhun. Thirties people were killed, 102 people disappeared, and more than 400,000 Rai of agricultural land destroyed.

The effects of storm can be described below:

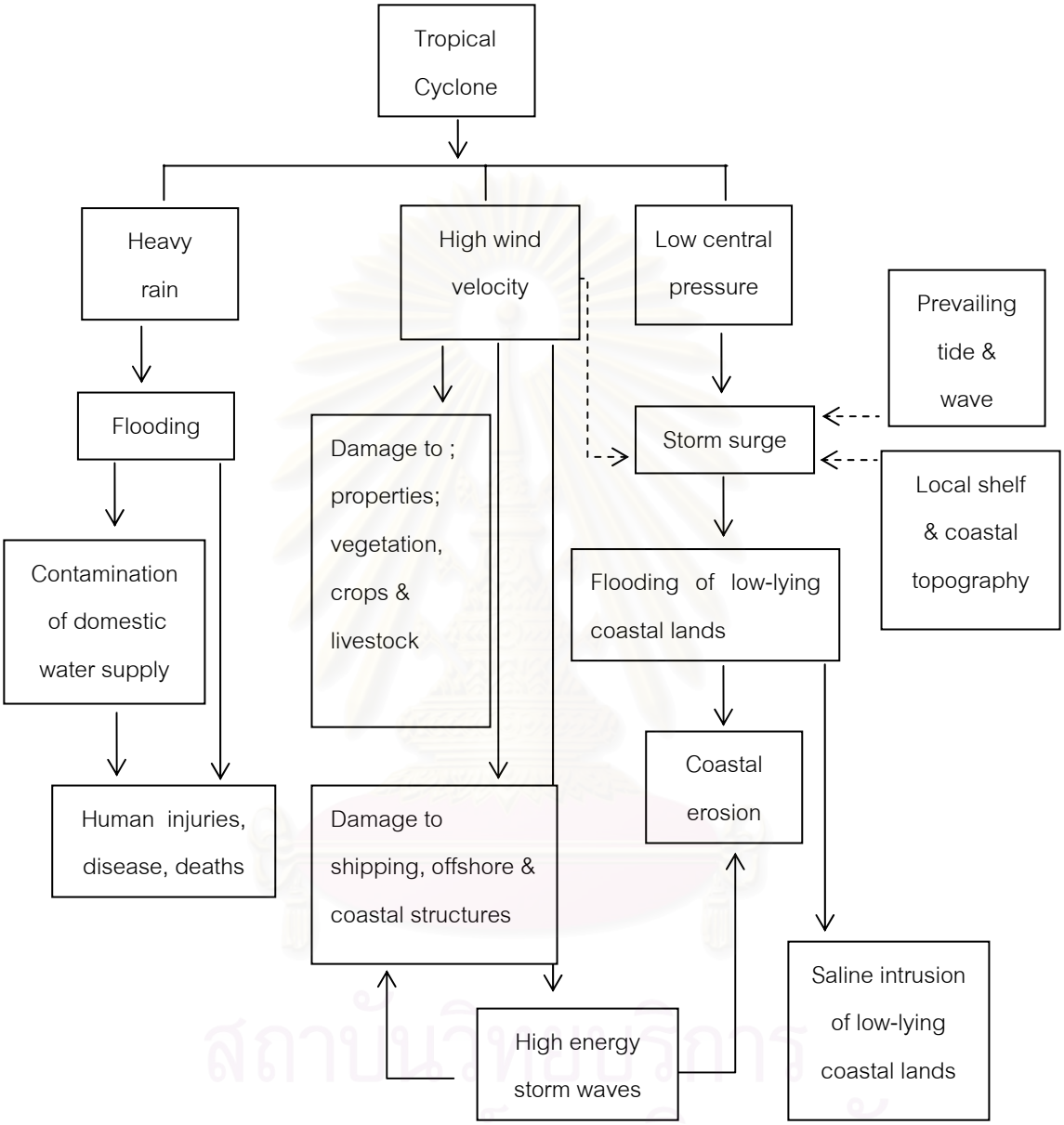

Figure 2.3 The impacts of tropical storm resulted directly from high winds, storm surge, heavy rain and flooding, and secondarily from the high energy storm waves generated by the winds from the tropical storm (Chapman,1994)

2.2.3 The storm surge models

The storm surge models have been utilized in many countries to provide useful information for warning system in those areas. For the Bay of Bengal, Flather (1993) used the numerical modeling which solved the modified depth-averaged equation by considering the effect of tide, wind, and river flux to simulate and predict tidal and surge elevation. The SPLASH model (Jelesnianski 1972 cited in Flather, 1991) was used to forecast hurricane surges along the east coast of the United States. SPLASH model is now extended to compute sea, lake, and overland surges from hurricanes called "SLOSH" (Pugh, 1987). The couple of a third generation wave model based on the energy conservation equations, and a two-dimensional storm surge were used to investigate the interactions between wave and currents (Zhang and Li, 1995). Zecchetto *et al.* (1997) used a finite element hydrodynamic model to examine the effects of wind on the storm surge patterns in Venice Lagoon in the Adriatic Sea. The storm surge model based on the depth-integrated shallow water equation with wind-wave enhanced bottom friction was applied to the Northwest coast of Australia, (Tang *et al.*, 1996).

For the Gulf of Thailand, there were many researches focusing on the effects of storm on the magnitude and direction of current (Wongwongchai, 1998; Schojolberg, 1998), and significant wave height (Kunbua, 1998; Akemahachai, 1998). Wongwongchai (1998) used the shallow water equation hydrodynamic model to simulate the current during the passage of Typhoon Gay in 1989. Unfortunately, there were no observed data to validate the model results. SEAWACTH program, a two- dimensional model, was forced by typhoon Linda wind and tide to investigate the circulation patterns (Schojolberg, 1998). The results did not correspond with the observed data. In 1998, Wave model (WAM) was used to simulate the significant wave height in case of typhoon Linda (Kunbua, 1998). At present, the former WAM model has been developed into an operation system to forecast significant wave height (Akemahachai, 1998). In addition, POM was used to develop storm surge model (not including tidal effect) for the Gulf of Thailand (May, 2003). However, there is no numerical model in operation to forecast sea surface elevation and current for warning the people who live in the risky area.

There are two and three dimensional models for storm surge simulation. For the coastal area, both models solved the shallow water equations to simulate the current, sea surface elevation, and significant wave height disturbed by storm. Princeton Ocean Model (POM) which was developed by Blumberg and Mellor in 1987, is a three-dimensional and fully non-linear ocean circulation model using realistic topography. It was used to simulate the circulation at various place such as the Straits of Florida (Mooers *et al.*, 1996), the west coast of Vancouver Island (Holloway *et al*., 1996), Gulf of Maine (Chai *et al.*, 1999), and Bangpakong Estaury (Buranapratheprat *et al*.,2003). Moreover, these models were applied to investigate the other phenomena, such as thermohaline structure of the South China Sea (Chu, 2001), spatial and temporal eddies in the Gulf of Thailand (Singharuck, 2002), and suspended sediment transport in Malacca Strait (Chan *et al.*, 2002). POM is also implemented to study the effects of storm in many countries, for instance, hurricane Andrew in the Gulf of Mexico (Keen, 1998), and hurricane Fran in 1996 at North Carolina (Wu *et al.*, 2002). POM has been used to simulate storm surge in the Gulf of Thailand using only atmospheric and wind forcing on the surface (May, 2003). The result cannot be compared with the sea surface elevation at tide gauge stations because tidal forcing was left out from the model.

In summary, storm surge models have been used to simulated storm phenomena in many regions of the world, but the accuracy of the simulations depends on accurate inputs as forcing functions. Additionally, the observation data were the most important to validate the model results.

CHAPTER 3

METHODOLOGY

In this chapter, the basic equations (governing equations) of numerical modeling were described first. Then, the applications of the model to the Gulf of Thailand were illustrated.

3.1 Numerical Modeling

Princeton Ocean model (POM), developed by Blumberg and Mellor in1987, is a two- and three-dimensional hydrodynamic model. It can simulate the flow and sea surface height in coastal ocean (e.g., HOLLOWAY, 1996; Mooers *et al.*, 1996; Xue *et.al*, 1999) estuaries (Buranapratheprat. *et al*, 2003), and river. Moreover, it can produce realistic bottom boundary layers which are important in coastal region when scheme is employed (cited in Mellor 2002, 1985).

3.1.1 Basic equations

The basis of the circulation model is the momentum conservation equation, and the continuity equation. Moreover, thermodynamic properties have been implemented, and the stratification of salinity and temperature are considered in the form of the energy equation, the salt equation, the turbulent energy equation, and the equation of state. These equations were solved in Cartesian coordinate on horizontal plane. All the equations were explained in the following section. To keep the number of depth layers constant across the entire study domain, sigma coordinate has been employed.

Derivation of the sigma coordinate equations is based on the transformation,

$$x = x \quad , \quad y = y \ , \quad \sigma = \frac{z - \eta}{H + \eta} \quad , \quad t = t \tag{3.1}$$

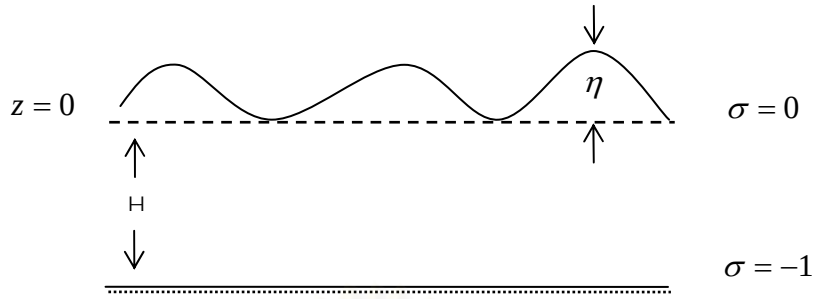

Figure 3.1 The vertical profile through the water column of the sigma coordinate system

Where x is coordinate in the east-west direction.

y is coordinate in the north-south direction.

z is a reference level of undisturbed surface. $z = 0$

$H(x, y)$ is the water depth at still water.

$\eta(x, y)$ is the surface elevation from reference level.

D is the total water depth ; $D \equiv H + \eta$.

$\sigma = 0$ is the water surface while $\sigma = -1$ is the bottom.

3.1.1.1 The continuity equation

Naturally, the net flux of water into or out of an area must be balanced by a corresponding change in the water level (Pugh, 1987).

$$\frac{\partial DU}{\partial x} + \frac{\partial DV}{\partial y} + \frac{\partial \omega}{\partial \sigma} + \frac{\partial \eta}{\partial t} = 0 \qquad (3.2)$$

where U and V are velocity component in $x-$and $y-$direction respectively.

ω is velocity in vertical component.

3.1.1.2 The momentum equation or equation of motion

The equation of motion was based on Newton's second law of motion, which stated that the changing rate of the momentum of the element is equal to the net force acting on the element.

In nature, the flows in the ocean are turbulent, changing in space and time. Therefore, time-averaging quantities (e.g., velocities, stress) were considered in this equation (Weiyan, 1992).

$$\frac{\partial UD}{\partial t}+\frac{\partial U^2D}{\partial x}+\frac{\partial UVD}{\partial y}+\frac{\partial U\omega}{\partial \sigma}-fVD+gD\frac{\partial \eta}{\partial x}+\frac{gD^2}{\rho_0}\int_{\sigma}^{0}\left[\frac{\partial \rho'}{\partial x}-\frac{\sigma'}{D}\frac{\partial D}{\partial x}\frac{\partial \rho'}{\partial \sigma'}\right]d\sigma'=\frac{\partial}{\partial \sigma}\left[\frac{K_M}{D}\frac{\partial U}{\partial \sigma}\right]+F_x \tag{3.3}$$

$$\frac{\partial VD}{\partial t}+\frac{\partial UVD}{\partial x}+\frac{\partial V^2D}{\partial y}+\frac{\partial V\omega}{\partial \sigma}+fUD+gD\frac{\partial \eta}{\partial y}+\frac{gD^2}{\rho_0}\int_{\sigma}^{0}\left[\frac{\partial \rho'}{\partial y}-\frac{\sigma'}{D}\frac{\partial D}{\partial y}\frac{\partial \rho'}{\partial \sigma'}\right]d\sigma'=\frac{\partial}{\partial \sigma}\left[\frac{K_M}{D}\frac{\partial V}{\partial \sigma}\right]+F_y \tag{3.4}$$

where f is the Coriolis parameter.

g is the gravitational acceleration (9.802 m/s^2).

$\frac{K_M}{D}\frac{\partial U}{\partial \sigma}$ and $\frac{K_M}{D}\frac{\partial V}{\partial \sigma}$ are turbulent stresses in x- and y- direction respectively.

K_M is the vertical kinematic viscosity.

ρ' is the fluctuated density.

F_x and F_y are horizontal viscosity terms which are defined as

$$F_x \equiv \frac{\partial}{\partial x}\left[H\tau_{xx}\right]+\frac{\partial}{\partial y}\left[H\tau_{xy}\right] \tag{3.4a}$$

$$F_x = \frac{\partial}{\partial x}\left[2H\left(A_M\frac{\partial U}{\partial x}\right)\right]+\frac{\partial}{\partial y}\left[HA_M\left(\frac{\partial U}{\partial y}+\frac{\partial V}{\partial x}\right)\right] \tag{3.4b}$$

$$F_y \equiv \frac{\partial}{\partial x}\left[H\tau_{xy}\right]+\frac{\partial}{\partial y}\left[H\tau_{yy}\right] \tag{3.4c}$$

$$F_y = \frac{\partial}{\partial x}\left[2H\left(A_M\frac{\partial V}{\partial y}\right)\right]+\frac{\partial}{\partial y}\left[HA_M\left(\frac{\partial U}{\partial y}+\frac{\partial V}{\partial x}\right)\right] \tag{3.4d}$$

where A_M and A_H are the horizontal viscosity and diffusivity coefficient respectively.

The Smagorinsky Diffusivity (1956, cited in Mellor, 2002) was employed to calculate the horizontal viscosity coefficient (A_M) using the equation below:

$$A_M = C\Delta x\Delta y\left[\left(\frac{\partial u}{\partial x}\right)^2 + \frac{1}{2}\left(\frac{\partial v}{\partial x}+\frac{\partial u}{\partial y}\right)^2 + \left(\frac{\partial v}{\partial y}\right)^2\right]^{1/2} \quad (3.5)$$

where C is the Smagorinsky Diffusivity coefficient.

Δx and Δy are grid spacing.

3.1.1.3 The energy equation

The energy equation was derived from the first law of thermodynamics which stated that the rate of energy change of the fluid particle was equal to the rate of heat added to the fluid particle plus the rate of work done on the particle (Versteeg and Malalasekera, 1995). The energy equation is given by

$$\frac{\partial \theta D}{\partial t}+\frac{\partial \theta UD}{\partial x}+\frac{\partial \theta VD}{\partial y}+\frac{\partial \theta \omega}{\partial \sigma}=\frac{\partial}{\partial \sigma}\left[\frac{K_H}{D}\frac{\partial \theta}{\partial \sigma}\right]+F_\theta-\frac{\partial R}{\partial z} \quad (3.6)$$

where θ is the potential temperature.

K_H is the vertical diffusivity.

$\left[\frac{K_H}{D}\frac{\partial \theta}{\partial \sigma}\right]$ is the vertical heat diffusitivity.

F_θ is the horizontal diffusitivity which is defined as

$$F_\theta \equiv \frac{\partial}{\partial x}\left[HA_H\frac{\partial \theta}{\partial x}\right]+\frac{\partial}{\partial y}\left[HA_H\frac{\partial \theta}{\partial y}\right] \quad (3.6a)$$

3.1.1.4 The salt diffusion equation

According to the conservation of salt, salt is transported by horizontal and vertical advections as described below:

$$\frac{\partial SD}{\partial t}+\frac{\partial SUD}{\partial x}+\frac{\partial SVD}{\partial y}+\frac{\partial S\omega}{\partial \sigma}=\frac{\partial}{\partial \sigma}\left[\frac{K_H}{D}\frac{\partial S}{\partial \sigma}\right]+F_S \quad (3.7)$$

Where S is salinity.

$\left[\frac{K_H}{D}\frac{\partial S}{\partial \sigma}\right]$ is the vertical salt diffusion term.

F_s is the horizontal diffusion term which is defined as

$$F_s \equiv \frac{\partial}{\partial x}\left[HA_H \frac{\partial S}{\partial x}\right] + \frac{\partial}{\partial y}\left[HA_H \frac{\partial S}{\partial y}\right] \tag{3.7a}$$

The turbulent stress and turbulent heat ($\frac{K_H}{D}\frac{\partial \theta}{\partial \sigma}$) and salt fluxes ($\frac{K_H}{D}\frac{\partial S}{\partial \sigma}$) were computed using the turbulent closure scheme (level 2.5 model), developed by Mellor and Yamada (1982) cited in Mellor (2002).

3.1.1.5 The turbulent energy equation

$$\begin{aligned}&\frac{\partial q^2 D}{\partial t} + \frac{\partial U q^2 D}{\partial x} + \frac{\partial V q^2 D}{\partial y} + \frac{\partial \omega q^2}{\partial \sigma} = \frac{\partial}{\partial \sigma}\left[\frac{K_q}{D}\frac{\partial q^2}{\partial \sigma}\right] + \\ &\frac{2K_M}{D}\left[\left(\frac{\partial U}{\partial \sigma}\right)^2 + \left(\frac{\partial V}{\partial \sigma}\right)^2\right] + \frac{2g}{\rho_0}K_H \frac{\partial \tilde{\rho}}{\partial \sigma} - \frac{2Dq^3}{B_1 l} + F_q\end{aligned} \tag{3.8}$$

$$\begin{aligned}&\frac{\partial q^2 l D}{\partial t} + \frac{\partial U q^2 l D}{\partial x} + \frac{\partial V q^2 l D}{\partial y} + \frac{\partial \omega q^2 l}{\partial \sigma} = \frac{\partial}{\partial S}\left[\frac{K_q}{D}\frac{\partial q^2 l}{\partial \sigma}\right] \\ &+ E_1 l\left[\frac{K_M}{D}\left[\left(\frac{\partial U}{\partial \sigma}\right)^2 + \left(\frac{\partial V}{\partial \sigma}\right)^2\right] + E_3 \frac{g}{\rho_0}K_H \frac{\partial \tilde{\rho}}{\partial \sigma}\right]\tilde{W} - \frac{Dq^3}{B_1} + F_l\end{aligned} \tag{3.9}$$

where l is the turbulence length scale.

q^2 is twice the turbulence kinetic energy.

B_1 is the turbulent constant (B_1=16.6).

3.1.1.6 The equation of state

This equation states that the density of water depends on salinity and potential temperature, which is given by

$$\rho = \rho(\theta, S) \tag{3.10}$$

Detail of the equation is given in Appendix A.

3.1.2 Boundary conditions

3.1.2.1 Surface and bottom boundary conditions

The perpendicular velocities were set to zero at the surface and the bottom. The wind stress was used as the surface stress and exerted on the surface of the model at every grid point.

$$\frac{K_M}{D}\frac{\partial}{\partial\sigma}(u,v) = \frac{1}{\rho_0}\left(\tau_{sx,}\tau_{sy}\right) \tag{3.11}$$

where $\left(\tau_{sx}, \tau_{sy}\right)$ is the wind stresses calculated as:

$$\left(\tau_{sx}, \tau_{sy}\right) = \rho_a C_W |W| W \tag{3.12}$$

where ρ_a is the air density.

C_W is the drag coefficient.

W is the calculated velocity:

$$W = \sqrt{u^2 + v^2} \tag{3.13}$$

where u and v are the component of velocities in x and y- direction at the specific height (10 m), respectively.

The bottom boundary conditions are

$$\frac{K_M}{D}\frac{\partial}{\partial\sigma}(u,v)=\frac{1}{\rho_0}(\tau_{bx,}\tau_{by}) \tag{3.14}$$

where (τ_{bx},τ_{by}) are the bottom stresses which are calculated as:

$$(\tau_{bx},\tau_{by})=C_Z\sqrt{u^2+v^2}(u,v) \tag{3.15}$$

where u and v are the component of velocities in x and y- direction respectively.

$$C_z=MAX\left[\frac{\kappa^2}{\left[\ln\left\{(1+\sigma_{kb-1})H/Z_0\right\}\right]^2},0.0025\right] \tag{3.16}$$

C_z is the bottom drag coefficient. κ is the Von Karman constant (0.4) and z_0 is the roughness parameter.

The boundary conditions for heat and salt equations are defined as heat flux(Q_θ) and salinity flux(Q_s).

Surface boundary : $$\frac{K_H}{D}\frac{\partial}{\partial\sigma}(\theta,S)=(Q_{\theta,}Q_S) \tag{3.17}$$

Bottom boundary : $$\frac{K_H}{D}\frac{\partial}{\partial\sigma}(\theta,S)=0 \tag{3.18}$$

The boundary conditions for turbulent energy equations are:

Surface boundary : $$q^2=B_1^{2/3}u_{\tau s}^2 \quad q^2l=0 \tag{3.19}$$

Bottom boundary : $$q^2=B_1^{2/3}u_{\tau b}^2 \quad q^2l=0 \tag{3.20}$$

where $u_{\tau s}$ and $u_{\tau b}$ are the friction velocity at the surface and bottom respectively.

3.1.2.2 Open boundary conditions

The tangential velocities at the defined open boundaries (details in section 3.4.2) were set to zero. The prescribed tidal current and elevation were used to calculate the vertically integrated, perpendicular velocities forced at the defined open boundaries according to gravity wave radiation condition (Flather, 1988).

$$U_n = \hat{U}_n \pm \frac{C}{H}\left(\eta - \hat{\eta}\right) \tag{3.21}$$

where $\hat{U}_n$ and $\hat{\eta}$ are input current and elevation respectively. C is shallow water wave speed which is given by $\sqrt{gH}$.

3.1.2.3 Coastal boundary conditions

The perpendicular velocity to any solid boundary is set to zero. A free-slip condition is applied on coastal boundaries by setting the tangential velocity gradient normal to the boundary to zero.

3.1.3 Numerical scheme

POM uses the horizontal finite difference scheme, staggered on a rectilinear coordinate system called an Arakawa C-grid. The atmospheric pressure is forced at the center of each cell, and the velocities are forced at the face of the cell as illustrated in Appendix B.

The model has a split time step for the external and internal mode to reduce the computation time. The external mode uses a short time step and external wave speed, while the internal mode uses a longer time step and internal wave speed. Both of the external and internal mode use time step based on the CFL condition (details in Appendix C). The time step for calculating the variables in the internal mode is separated into a vertical diffusion time step (implicit) to accommodate small vertical spacing near the surface, and an advection plus horizontal diffusion time step (explicit).

The external mode provides the vertically averaged velocities and sea surface elevation for internal mode to calculate the independent (vertical) velocity, thermal properties (temperature, and salinity), and turbulent quantities.

3.2 Model application to the Gulf of Thailand

3.2.1 Model domain

The model domain for the Gulf of Thailand extends from latitude 3º-14º N and longitude 99º-109º E as shown in Figure 3.2. A horizontal grid resolution of 0.1 degree (about 11.1 km) was used in the model. Therefore, the grids consisted of 101x111 cells. Twenty one levels in sigma coordinate were used in vertical resolution. This domain occupied the Gulf of Thailand and extended into the South China Sea to track the movement of storm surge before passing through the Gulf of Thailand.

3.2.2 Bathymetry

Bathymetry was extracted from NOAA National Geophysical Data Center ETOPO5 database which have the resolution of 5'×5' (10x10 km) horizontally.

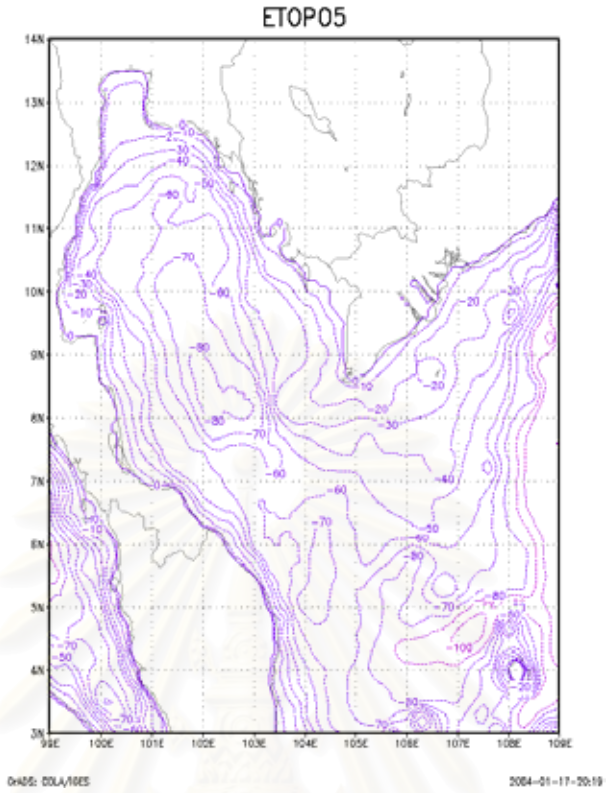

Figure 3.2 Bathymetry of the Gulf of Thailand form ETOPO5

3.2.3 Temperature and salinity

Temperature and salinity was initialized by interpolating from 1-degree resolution climatography data (Levitus *et al.,* 1994).

3.2.4 External forcing function

3.2.4.1 Meteorological data (wind and pressure fields)

Wind and pressure data were obtained from the U.S. Navy Global Atmospheric Prediction System (NOGAPS), a global atmospheric forecast model with approximately 1º (about 110 km) grid spacing. The forcing fields were obtained from the Master Environmental Library (MEL). But these data are not available on the model grids, so the bilinear interpolation was used to interpolate the data set of 1ºx1º grid to 0.1ºx0.1º grid.

3.4.2.2 Tidal forcing

Tidal elevation and current at the eastern and southern boundaries (defined open boundaries) were derived from Oregon State University (OSU) Tidal Inversion Software (OTIS) regional scale (1/6º) model of Indonesian Seas (Egbert and Erofeeva, 2002) in the form of harmonic constants. This software analyzes the sea surface elevation from altimeter which is the sensor on TOPEX/POSEIDON satellite. Eight principal tidal constituents, composed of four diurnal tides (K_1, O_1, Q_1, P_1) and semi-diurnal tides (M_2, S_2, K_2, N_2), were used to compute tidal elevation by the following equation.

$$h(t) = \sum A_i \cos[(V_o + u)_i + \sigma_i t - \kappa_i] \qquad (3.22)$$

where κ_i = the phase lag behind equilibrium for constituent i

$(V_0 + u)_i$ = nodal factor

σ_i = phase increment per mean solar hour of each constituent (detail in Appendix D)

A_i = the amplitude of constituent i

Tidal elevation is then used to compute tidal current (3.22) at the prescribed boundaries and the current is used to drive the tidal model.

3.2.5 Details of numerical experiments

Parameters used in this study were described below:

Density of water	1025 kg/m^3
Density of air	1.03 kg/m^3
Smagorinsky diffusivity coefficient	0.01
Bottom roughness	0.01
Internal time step	10 minutes
External time step	10 seconds

3.2.6 Model verification

Experiment I : Model response to co-oscillation tide

To investigate the effect of tide on sea surface elevation, the model was driven by only co-oscillation tide at the open boundaries. The calculated tidal elevation from the model in 1997 were then compared with hourly time series of the elevation at 4 tide gauges maintained by the Hydrographic Department, Royal Thai Navy , namely Ko Lak, Ko Prab ,Ko Mattapone ,and Leam Singha station (see figure D.1 in Appendix D) , and results from the tidal model (OTIS) from Oregon State University. The calculated tidal elevation was analyzed to retrieve amplitude and phase of those constituents by using harmonic analysis package developed by Japan Oceanographic Data Center (JODC).

Experiment II : Model response to a combination of meteorological forcing and co-oscillation tide

The purpose of this experiment is to examine the interaction between tide and surge, and simulate the sea surface elevation disturbed by tropical storm “Linda“ in 1997. The model was driven by the combination of the meteorological data (wind and pressure), which were exerted on the surface of the model, and co-oscillation tide at the open boundaries. Wind and pressure data came in the form of 12-hours forecast starting from 21st October to 10th November 1997. The hourly time series of calculation of sea surface height were compared with the observed values at the tide gauges.

Experiment II was designed into 4 sub-experiments using different surface drag coefficients. (C_w in equation(3.12))

Experiments	Drag coefficient (C_W)		
A	$C_W = (0.63 + 0.066 * W) * 10^{-3}$		
B	$C_W = 0.0011$	for	W < 6 m/s
	$C_W = (0.61 + 0.063 * W) * 10^{-3}$	for	$6 \le W \le 22$ m/s
	$C_W = (1 + 0.07 * W) * 10^{-3}$	for	W >22 m/s
C	$C_W = 1 * 10^{-3}$	for	W < 7 m/s
	$C_W = (0.1923 + 0.1154 * W) * 10^{-3}$	for	$7 \le W \le 20$ m/s
	$C_W = 2.5 * 10^{-3}$	for	W>20 m/s
D	$C_W = (0.63 + (0.066 * W^2)^{1/2}) * 10^{-3}$		

Experiment III : Model verification with other storms

The model obtained from experiment II was verified with other typhoons that passed through the Gulf, namely Gil and Chip. Their wind and pressure data covered the period from November 10, 1998 to November 30, 1998, and December 3, 1998 to December 20, 1998 respectively. In this experiment, only sea surface elevation was considered since measured current data were not available to verify the model results.

CHAPTER 4

RESULTS AND DISCUSSIONS

Experiment I : Model response to co-oscillation tide

Observed values of harmonic constants (amplitudes and phases) of the four principal constituents; M_2, S_2, K_1, and O_1 tides at 23 tide gauges were compared with those calculated from the model results as illustrated in Figure 4.1 and table 4.1.

The amplitude comparison showed very good agreement for K_1, O_1 (diurnal tides) and S_2 (semi-diurnal tide). For M_2 (semi-diurnal tide), the model underpredicted the observed values by 10-20 cm. The reason for this is that our model cannot generated seiche caused by M_2 at the Upper Gulf (Yanagi, 1997). The Root Mean Square Error is 18.23, 4.45, 4.94, and 3.76 cm for M_2, S_2, K_1, and O_1 tides respectively. For phase comparison, the model provided good agreement for M_2, K_1 and O_1. The phase of K_1 from the model leads and lags the observed values by 60 degree while the phase of S_2 from the model lags the observed values by 90 degree. The phase of O_1 lags the observed values by about 30 degree.

When comparing with OTIS results (Figure 4.2), the hydrodynamic model of the Gulf of Thailand underpredicts the amplitudes and phases for M_2 tide by about 10 cm, and 180 degrees respectively. Phase of K_1 and O_1 of POM lead the OTIS phases by around 90 degrees. The discrepancy in amplitudes and phases of S_2 exist in some stations located on the eastern of the Gulf (see Figure 4.2).

The obtained amplitudes of M_2 tide from the hydrodynamic model were less than those from tide gauges. This may be accounted for by the underpredicted tidal inputs from TOPEX/POSEIDON at the prescribed open boundaries (see Table 4.1).

The results from both models and tidal gauges illustrated that the amplitudes of K_1 tide were larger than those of M_2 tide because of the natural oscillating period (T_n). In fact, T_n can be expressed as:

$$T_n = 4L/\sqrt{gh} \quad (4.1)$$

where L is the length of the Gulf of Thailand (around 500 km), h is the mean depth of the Gulf (about 57.4 m). So, T_n for the Gulf of Thailand is 23.42 hours which is near the diurnal period (see Appendix E).

The Form number (F) was used to indicate the tidal type at each place (Johnstons, 1998) and was expressed as: (see Table 4.2)

$$F = \frac{K_1 + O_1}{M_2 + S_2} \quad (4.2)$$

Form number	Tidal type
F < 0.25	Semi-diurnal tide
0.25 < F < 1.50	mixed tide; mainly semi-diurnal tide
1.50 < F < 3.00	mixed tide; mainly diurnal tide
F > 3.00	diurnal tide

The discrepancy of computed form number exists at Sattahip, Hua Hin, Pran Buri, Klong Yai, Langsuan, Ko Prab, and Sichol stations due to low M_2 amplitude from the model results.

The tidal range, which is the difference in heights between consecutive high and low waters, of model output, field observation, and OTIS are list in Table 4.3. It showed that the tidal ranges obtained from POM were higher than those from tide gauges at nearly all stations.

Tidal range = mean high water – mean low water

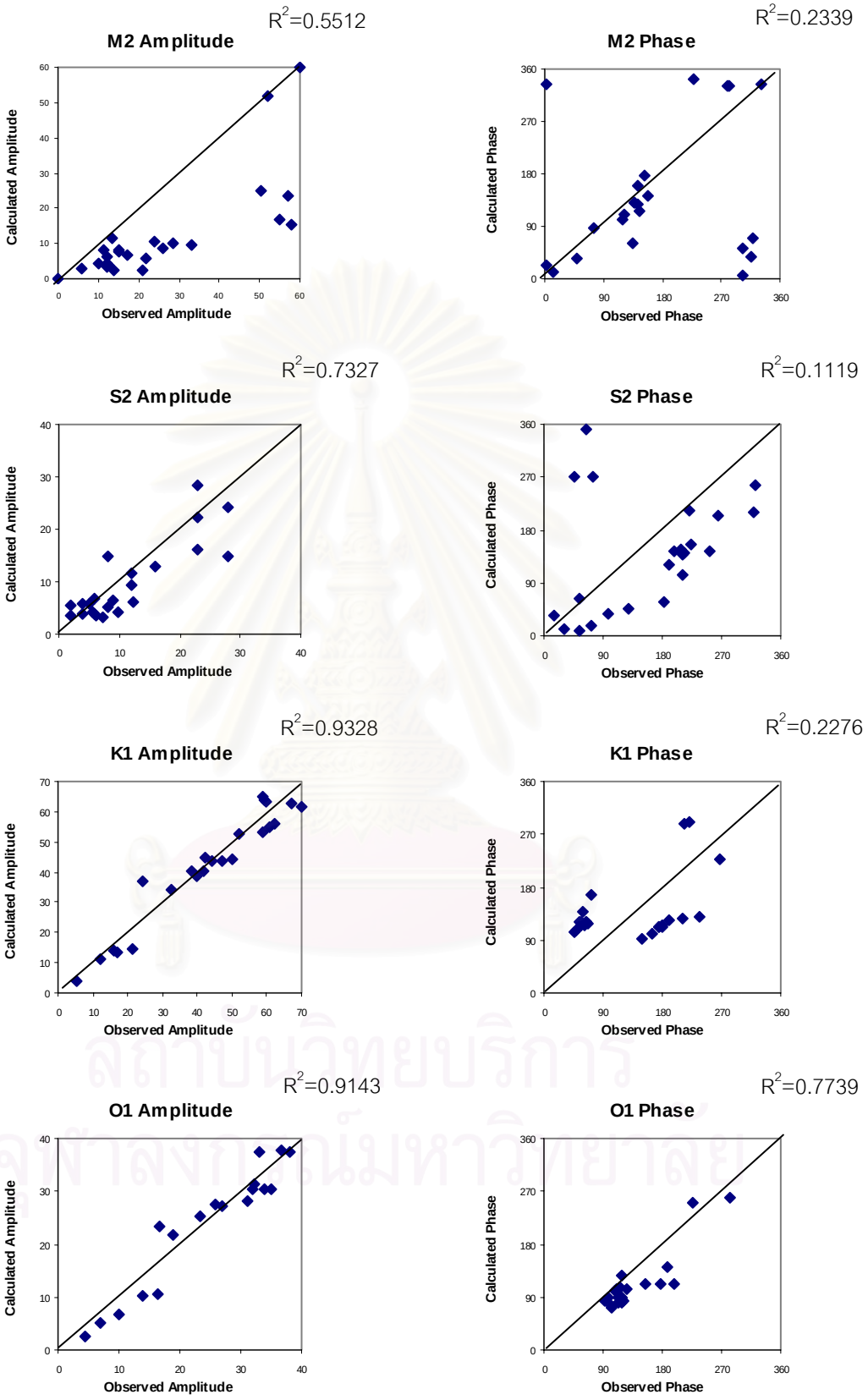

Figure 4.1 Scatter diagrams for the amplitude (in cm) and phase (in degree) between the elevations from the observed values and the hydrodynamic model for M_2, S_2, K_1, and O_1

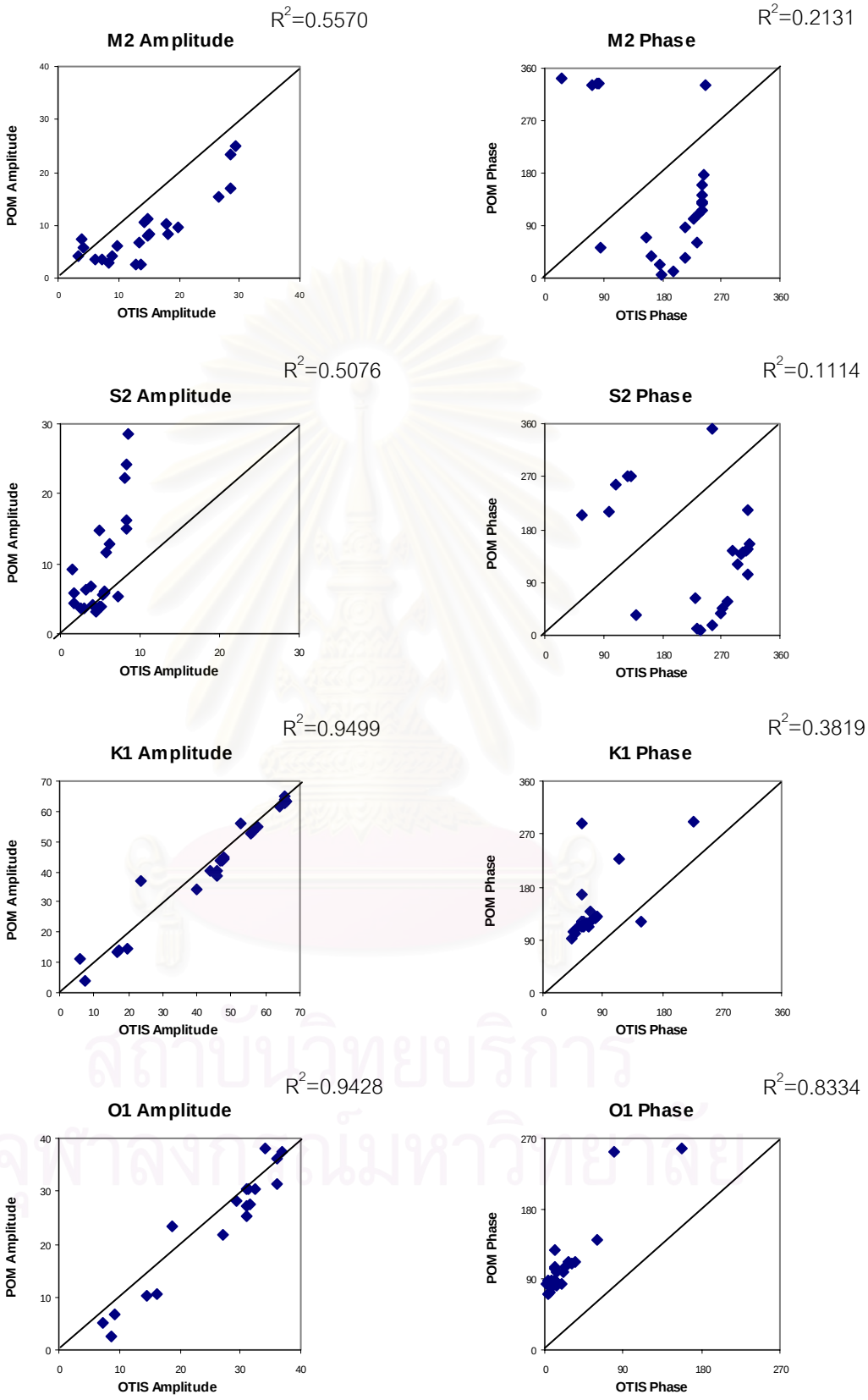

Figure 4.2 Scatter diagrams for the amplitude (in cm) and phase (in degree) between the elevations from the hydrodynamic model and OTIS model for M_2, S_2, K_1, and O_1

Table 4.1 Comparison of observed and calculated harmonic constants of 4 principal constituents M_2, S_2, O_1, K_1

Stations	M_2						S_2						K_1						O_1					
	Amplitude			Phase			Amplitude			Phase			Amplitude			Phase			Amplitude			Phase		
	Obs.	OTIS	POM	Obs.	OTIS	POM	Obs.	OTIS	POM	Obs.	OTIS	POM	Obs.	OTIS	POM	Obs.	OTIS	POM	Obs.	OTIS	POM	Obs.	OTIS	POM
Klong Yai	12.7	6.2	3.6	3.3	176	23.1	6.1	2.6	3.7	63.4	257	351	32.8	40.1	34.2	149	42.6	93.1	19.0	27.2	21.7	92.4	1.72	83.5
Leam Ngob	12.0	7.3	3.5	14.0	198	12.7	9.0	3.1	6.4	73.0	257	17.8	42.0	43.9	40.3	45.0	44.8	104	31.0	29.4	28.2	103	3.17	72.1
Leam Singha	10.0	9.0	4.3	49.0	214	35.7	6.0	3.8	6.8	97.0	269	37.1	47.0	46.7	43.8	49.0	47.3	106	32.0	31.1	30.4	102	4.99	73.8
Prasae	12.1	9.8	6.1	74.9	216	86.8	5.5	4.0	4.1	128	271	47.4	42.2	47.8	44.9	164	47.3	99.5	25.9	31.7	27.4	97.3	4.77	88.5
Rayong	24.0	14.2	10.7	120	228	103	8.0	4.9	14.8	252	287	144	62.0	52.5	56.2	55.0	149	121	47.0	34.1	38.1	114	7.36	88.9
Ao Sattahip	26.0	18.3	8.4	121	235	110	12.0	5.8	11.5	191	296	122	59.0	56.0	53.3	56.0	55.7	114	42.0	36.0	36.3	112	9.68	82.0
Si chang	58.0	26.7	15.5	136	240	130	23.0	8.0	22.3	198	308	145	70.0	64.1	61.5	63.0	59.1	120	42.0	39.5	41.1	119	10.9	88.7
Bangpakong	52.0	29.1	51.9	159	241	142	23.0	8.6	28.5	222	311	212	60.0	66.2	63.3	71.0	59.8	167	39.0	40.3	43.0	118	11.1	128
Bangkok bar	55.0	28.5	16.9	138	242	132	28.0	8.4	24.3	209	311	147	67.0	65.7	62.8	56.0	60.1	121	45.0	40.2	42.2	118	11.5	89.6
Chulachomkla	57	28.6	23.3	145	242	117	28.0	8.4	15.0	212	311	103	59.5	65.8	63.8	176	60.1	113	38.1	40.3	37.3	110	11.5	103
Maeklong	50.2	29.4	25.0	153	243	176	23.0	8.4	16.2	223	313	155	58.7	65.7	64.8	179	61.2	116	36.6	40.2	37.7	115	12.3	106
Pranburi	28.4	17.9	10.2	143	241	159	12.3	5.5	6.1	211	301	138	52.2	55.9	52.9	175	59.4	111	32.3	36.0	31.5	107	12.8	99.8
Hua hin	33.0	19.9	9.5	143	241	127	16.0	6.1	12.9	214	303	142	61.0	57.6	54.9	63.0	59.3	120	33.0	36.8	37.3	117	12.5	87.8

Table 4.1 (continued) Comparison of observed and calculated harmonic constants of 4 principal constituents M_2, S_2, O_1, K_1

Stations	M_2						S_2						K_1						O_1					
	Amplitude			Phase			Amplitude			Phase			Amplitude			Phase			Amplitude			Phase		
	Obs.	OTIS	POM	Obs.	OTIS	POM	Obs.	OTIS	POM	Obs.	OTIS	POM	Obs.	OTIS	POM	Obs.	OTIS	POM	Obs.	OTIS	POM	Obs.	OTIS	POM
Langsuan	15.0	3.9	7.5	315	164	37.1	9.8	1.6	4.3	31.2	232	10.4	38.2	45.8	40.6	179	69.7	113	23.4	31.0	25.3	111	21.4	100
Ko Lak	6.0	8.3	3.0	134	232	61.3	2.0	3.0	3.6	182	280	58.4	50.0	48.0	44.0	62.0	60.3	115	34.0	32.5	30.5	117	14.3	81.9
Ko Mattapo	12.0	3.3	4.2	303	178	7.2	4.0	1.6	5.9	55.0	237	8.0	40.0	45.8	38.7	66.0	66.7	118	27.0	31.0	27.2	121	19.1	84.5
Ko Prab	22.0	4.3	5.9	318	156	69.3	12.0	1.5	9.2	54.0	231	64.4	44.0	47.5	43.5	59.0	71.9	138	35.0	31.2	30.3	126	23.5	105
Sichol	17.0	13.4	6.7	303	86.2	52.7	7.2	4.5	3.1	14.4	140	34.4	24.4	23.8	37.2	190	74.5	125	16.6	18.8	23.4	199	26.7	112
Paknakorn	15.1	14.8	8.0	331	82.9	335	6.0	4.8	3.8	46.8	132	272	21.5	19.5	14.3	212	78.7	128	16.4	16.1	10.7	154	31.2	111
Pakpanang	11.2	15.2	8.2	2.8	80.9	334	3.9	5.0	3.9	74.1	127	270	17.1	17.0	13.4	236	81.9	130	13.8	14.6	10.1	178	34.3	112
Songkhla	13.6	14.8	11.3	279	72.6	332	4.9	5.6	5.8	322	109	255	5.3	7.2	3.7	268	116	228	4.5	8.6	2.5	187	60.1	140
Pattani	21.0	12.9	2.6	283	247	332	2.0	5.4	5.5	320	98.2	210	12.0	6.1	11.4	213	59.3	288	7.0	7.2	5.1	226	79.8	252
Bang nara	14.0	13.8	2.5	228	27.1	342	8.0	7.3	5.3	264	57.2	204	16.0	17.3	13.8	222	228	291	10.0	9.1	6.7	282	158	258

Table 4.2 The form numbers (F) and tidal types calculated from tide gauge data and the hydrodynamic model results

Stations	Observation		Calculation	
	Form number	Type	Form number	Type
Klong Yai	2.76	Mixed	7.66	Diurnal
Leam Ngob	3.13	Diurnal	2.62	Mixed
Leam Singha	4.21	Diurnal	6.68	Diurnal
Presae	3.87	Diurnal	7.09	Diurnal
Rayong	3.41	Diurnal	3.70	Diurnal
Ao Sattahip	2.66	Mixed	4.50	Diurnal
Ko Si Chang	1.38	Mixed	2.71	Mixed
Bangpakong	1.32	Mixed	1.32	Mixed
Bangkok Bar	1.35	Mixed	2.55	Mixed
Chulachomkhlao Fort	1.15	Mixed	2.64	Mixed
Maeklong	1.30	Mixed	2.49	Mixed
Pranburi	2.08	Mixed	5.18	Diurnal
Hua Hin	1.92	Mixed	4.12	Diurnal
Langsuan	2.48	Mixed	5.58	Diurnal
Ko Lak	10.50	Diurnal	11.29	Diurnal
Ko Mattapone	4.19	Diurnal	6.52	Diurnal
Ko Prab	2.32	Mixed	4.89	Diurnal
Sichol	1.69	Mixed	4.89	Diurnal
Paknakorn	1.80	Mixed	2.12	Mixed
Pakpanang	2.05	Mixed	1.94	Mixed
Songkhla	0.53	Mixed	0.36	Mixed
Pattani	0.83	Mixed	2.04	Mixed
Bangnara	1.18	Mixed	2.63	Mixed

Table 4.3 The comparison of tidal ranges (in meter) among OTIS model, hydrodynamic model ,and tide gauge

Stations	Tidal Range		
	OTIS	POM	Tide guage
Klong Yai	1.48	1.26	1.00
Leam Ngob	1.58	1.47	1.15
Leam Singha	1.65	1.60	1.60
Prasae	1.70	1.44	1.22
Ko Sichang	2.33	2.50	1.80
Bangpakong	2.40	2.57	1.87
Bangkok Bar	2.39	2.57	2.44
Chulachomkhlao Fort	2.39	2.57	2.24
Maeklong	2.43	2.66	1.62
Pran buri	1.99	1.92	1.45
Hua hin	2.06	2.05	2.46
Langsuan	1.65	1.30	1.14
Ko Lak	1.74	1.55	1.88
Ko Mattapone	1.37	1.59	1.75
Ko Prab	1.67	1.67	2.09
Sichol	1.02	1.29	0.76
Paknakorn	0.97	0.71	0.62
Pakpanang	1.99	0.69	0.54
Songkhla	0.75	0.62	0.31
Bangnara	0.82	0.57	0.48

The hourly time series tidal elevation for 1997 among OTIS, hydrodynamic model (POM) output and the observed data, which had only eight tidal constituents (M_2, S_2, K_1, O_1, P1, Q_1, N_2, and K_2) were compared (see Figure 4.3(A) to 4.4(F)). The comparison of tidal elevations between the hydrodynamic model and OTIS model (Figure 4.3(A) to (E)) were described below:

The results showed that the elevation from the hydrodynamic model agree well with OTIS model at almost all stations as illustrated in Figure 4.3(A) to 4.3(E), except at Hua Hin station where the tidal elevation results from POM are higher than the values obtained form OTIS by about 0.5 m (see Figure 4.3(B)).

At Leam Singha station, the calculated tidal elevations are lower than the OTIS values by 10 cm in May, June, July, November, and December, whereas their values are higher than the OTIS results in March, August, and September. In February and April, the calculated values are equal to the observed values. The calculated phases are in phase in April, May, September, October, and November. In the other months, the calculated phases lead the observed phases by about 1 hour.

The tidal elevations from POM at Hua Hin station were resemble to the OTIS values in May, June, July, November, and December. In the other months, the models overpredicted the OTIS values.

At Ko Lak station, the model overestimates the tidal elevations when compared with OTIS results in February, March, April, August, September, and October. The calculated phases are in phase in most of the months, except in January, July, and August. Its phases lead the OTIS phases by around 1 hour.

At Ko Mattapone station, the calculated tidal elevations agree well with the tidal elevation obtained from OTIS, except in June, July, September, and December. The OTIS phases lag behind the model phases by about 1 hour in January, February, March, June, July, August, and December.

At Ko Prab station, the calculated tidal elevations are equal to the tidal elevations from OTIS in most of the months, except in March, June, September, and December especially during the neap tide. The calculated phases lead the OTIS phases by about 2 hours only in June, July, August, and December.

The correlation coefficients of POM and OTIS results are 0.69, 0.74, 0.81, 0.76, and 0.79 at Leam Singha, Hua Hin, Ko Lak, Ko Mattapone, and Ko Prab respectively.

The discrepancy between POM and OTIS seem to occur because of the difference in equations which are used to calculate the tidal elevation. In fact OTIS solved equation (3.22), whereas POM solved continuity to calculate these data.

The tidal elevation comparison between the observed values and the results from POM showed fairly good agreement for Leam Singha (Figure 4.4(A)), Ko Lak (Figure 4.4(C)), and Ko Mattapone (Figure 4.4(D)) station.

At Leam Singha station, POM provides a good agreement for the tidal elevations comparing with the tide gauge values except in September. In this month, the calculated tidal elevations are lower than the observed value by about 20 cm, and its phases lag the OTIS phases by about 2 hours. Phases of POM lead the tide gauge values in January, February, March, and April by around 1 hour.

At Hua Hin station, the plot showed that tide type of this station is mixed-tide; mainly semi-diurnal tide, whereas POM results indicated diurnal tide.

At Ko Lak station, the tidal elevations from POM agree well with the elevations from tide gauge in all months.

At Ko Mattapone station, the calculated tidal elevations are resemble to the the observed values but the discrepancy still exist during the neap tide in April, May, June, October, November, and December.

At Ko Prab station, the calculated tidal elevations are less than the observed values by about 20 cm. The tidal type of observed data is mixed tide; mainly semi-

diurnal tide while the tidal type from POM is diurnal tide. The discrepancy arose from inaccuracy of the model bathymetry which does not account for the presence of Ko Samui near Ko Prab station. In fact, the waters are confined in this area.

The correlation coefficients of POM and observed results are 0.73, 0.60, 0.84, 0.82, and 0.71 at Leam Singha, Hua Hin, Ko Lak, Ko Mattapone, and Ko Prab respectively.

In summary, the discrepancies in tidal elevations and phases between POM and observed values seem to occur because of the inaccuracy of the prescribed tide from TOPEX/POSEIDON at the open boundaries (see Table 4.1), shape and depth of the model area.

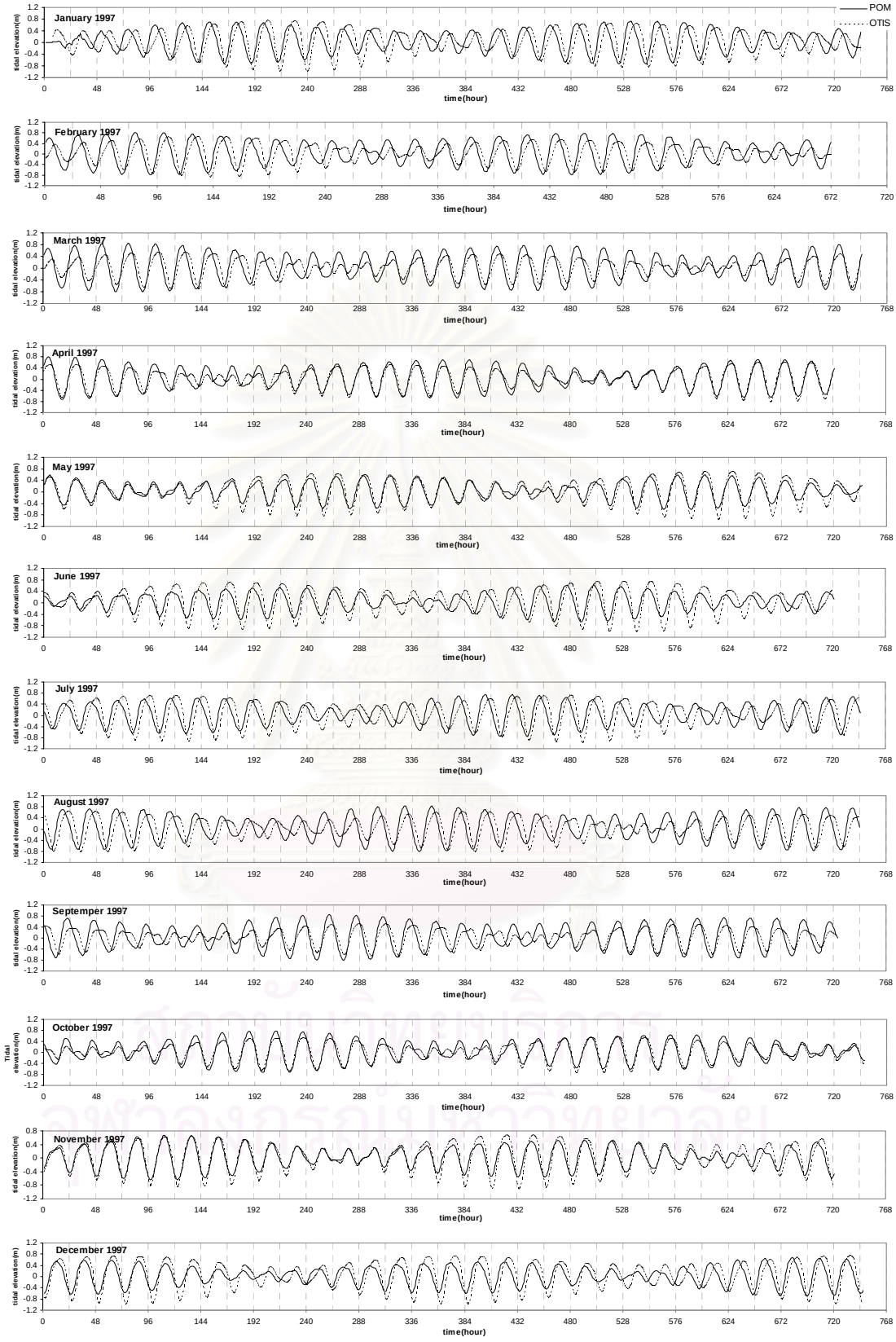

Figure 4.3(A) The comparison of the tidal elevation (in meters) between the hydrodynamic model based on POM and OTIS at Leam Singha station

Figure 4.3(B) The comparison of the tidal elevation (in meters) between the hydrodynamic model based on POM and OTIS at Hua Hin station

Figure 4.3(C) The comparison of the tidal elevation (in meters) between the hydrodynamic model based on POM and OTIS at Ko Lak station

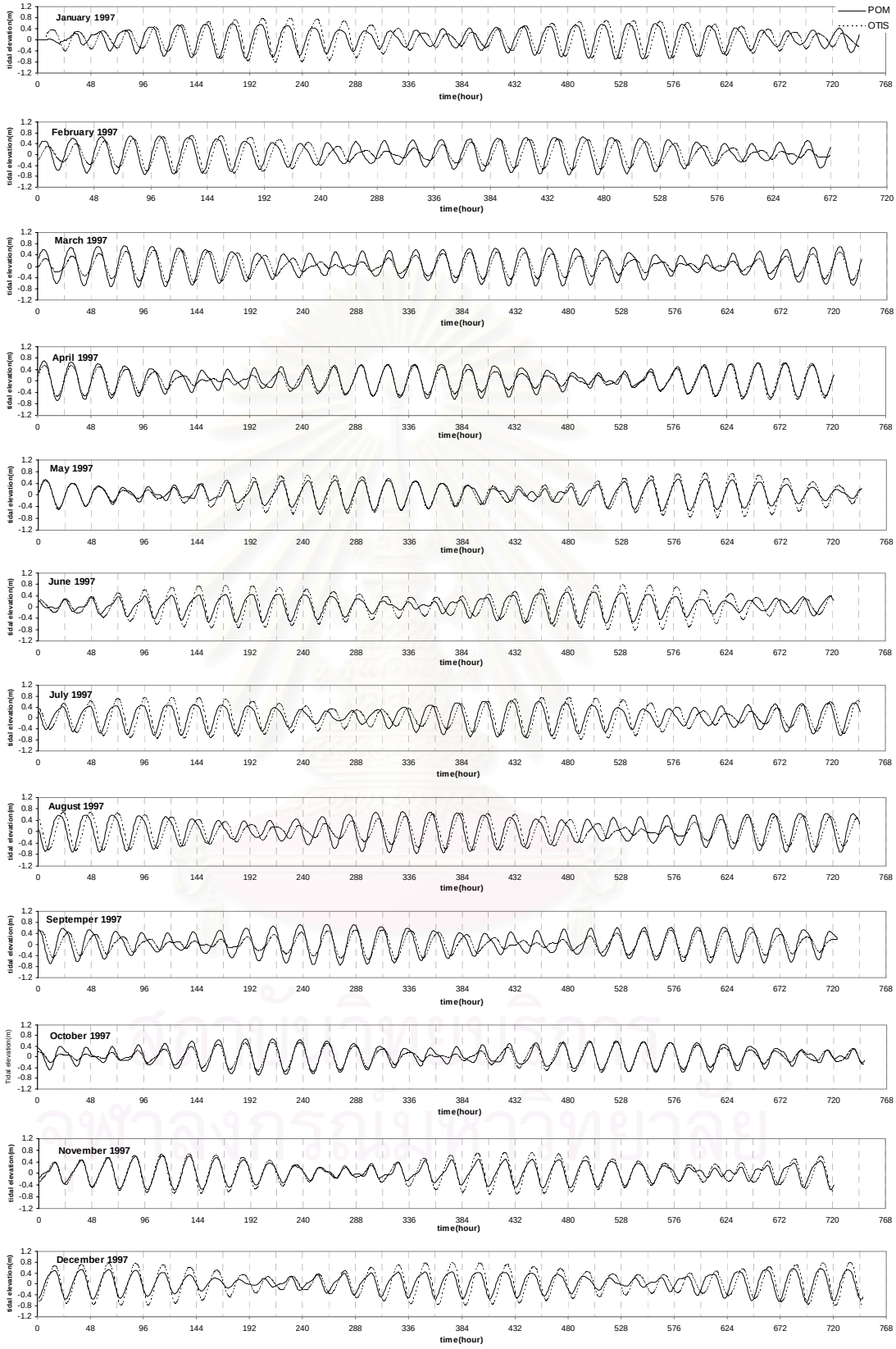

Figure 4.3(D) The comparison of the tidal elevation (in meters) between the hydrodynamic model based on POM and OTIS at Ko Mattapone station

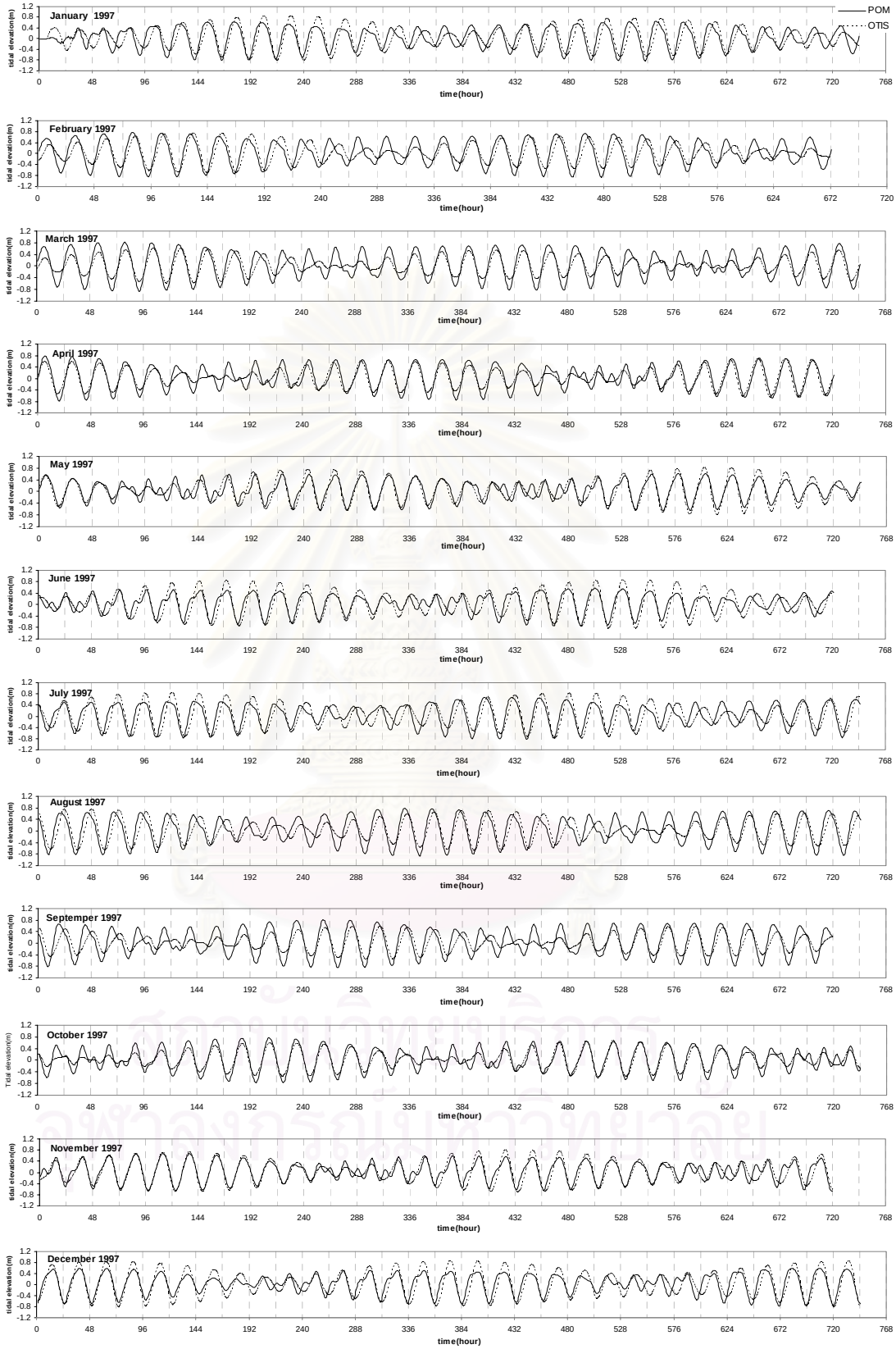

Figure 4.3(E) The comparison of the tidal elevation (in meters) between the hydrodynamic model based on POM and OTIS at Ko Prab station

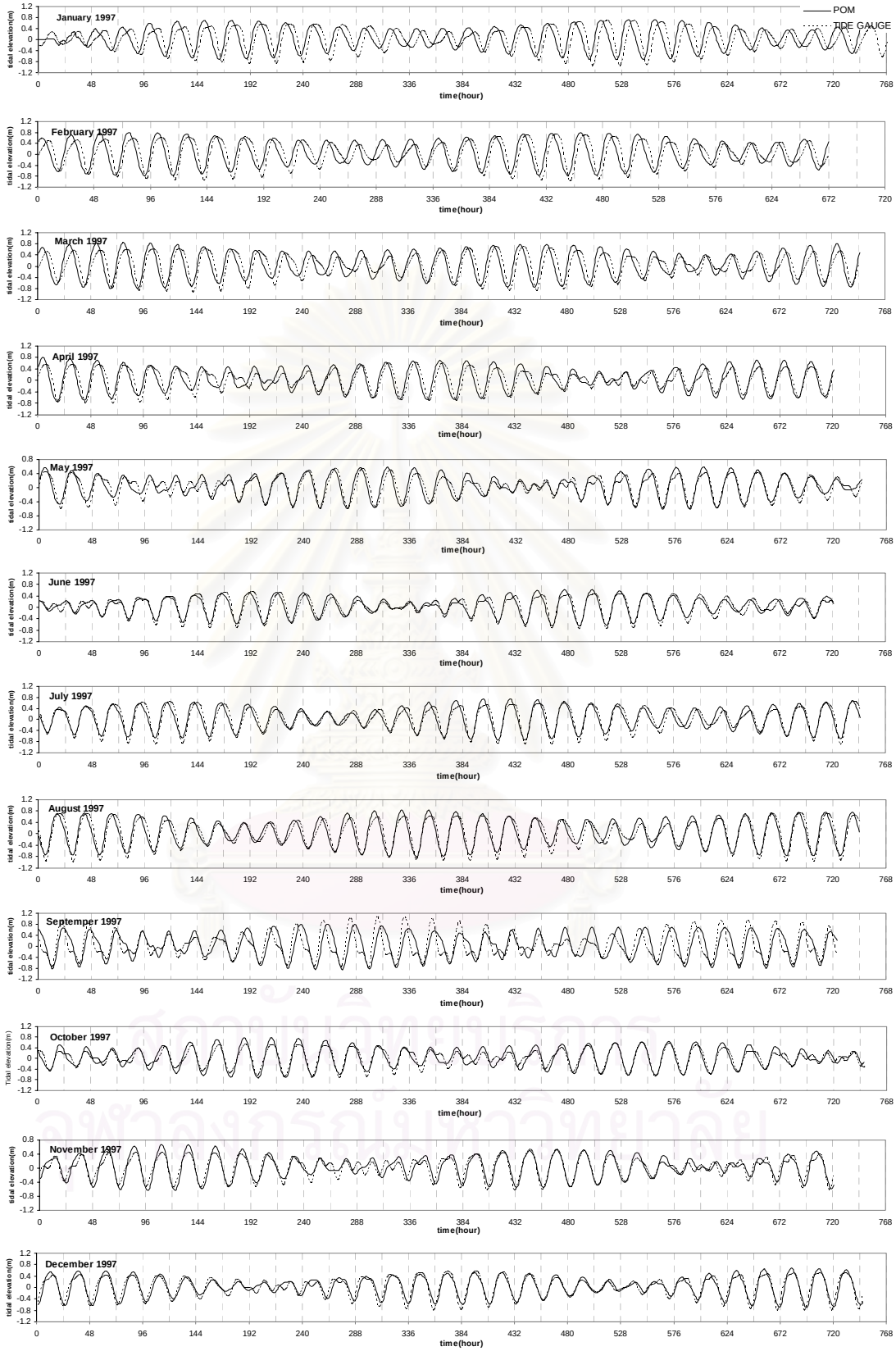

Figure 4.4(A) The comparison of the tidal elevation (in meters) between the hydrodynamic model based on POM and observed at Leam Singha station

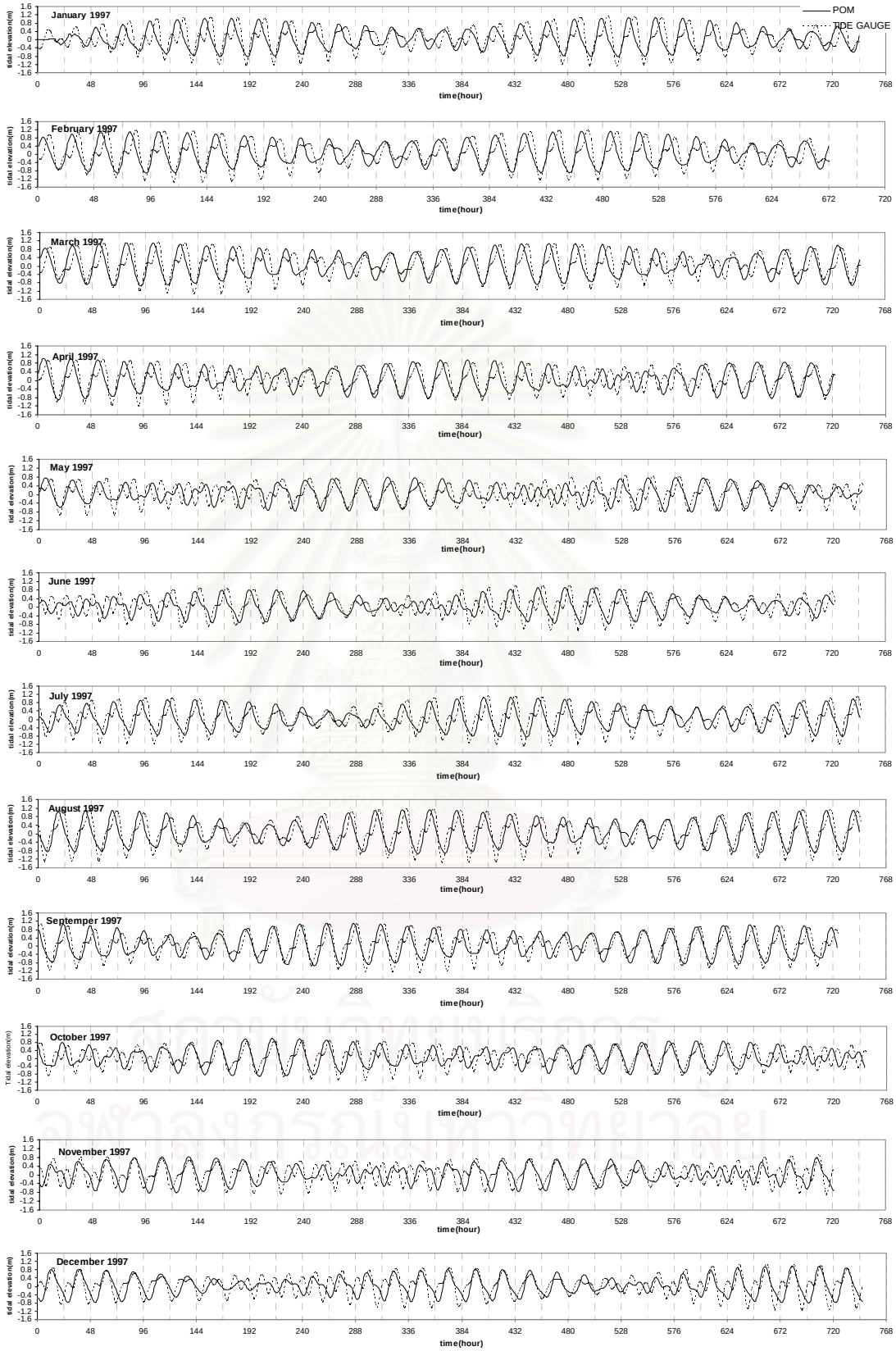

Figure 4.4(B) The comparison of the tidal elevation (in meters) between the hydrodynamic model based on POM and observed at Hua Hin station

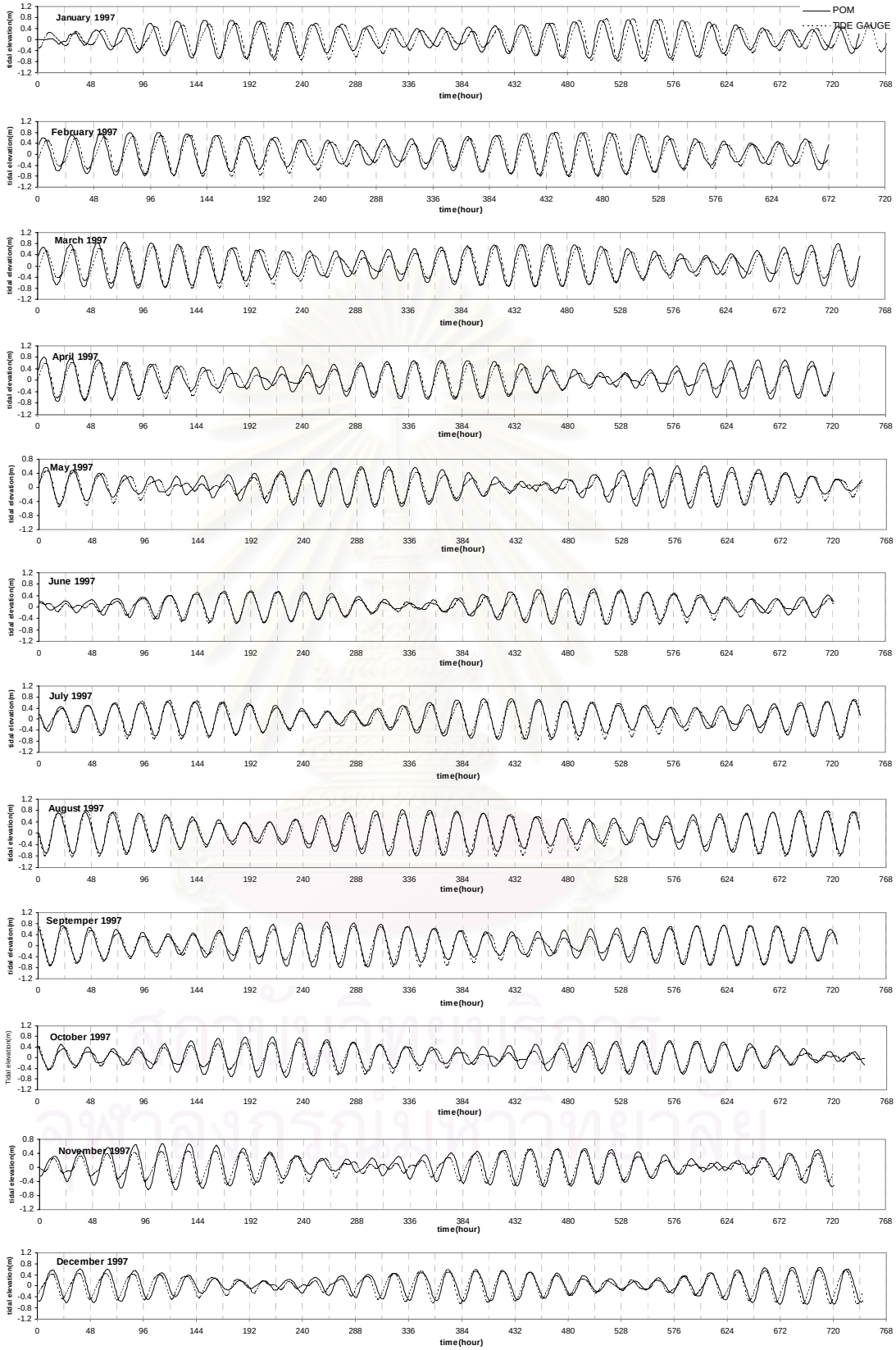

Figure 4.4(C) The comparison of the tidal elevation (in meters) between the hydrodynamic model based on POM and observed at Ko Lak station

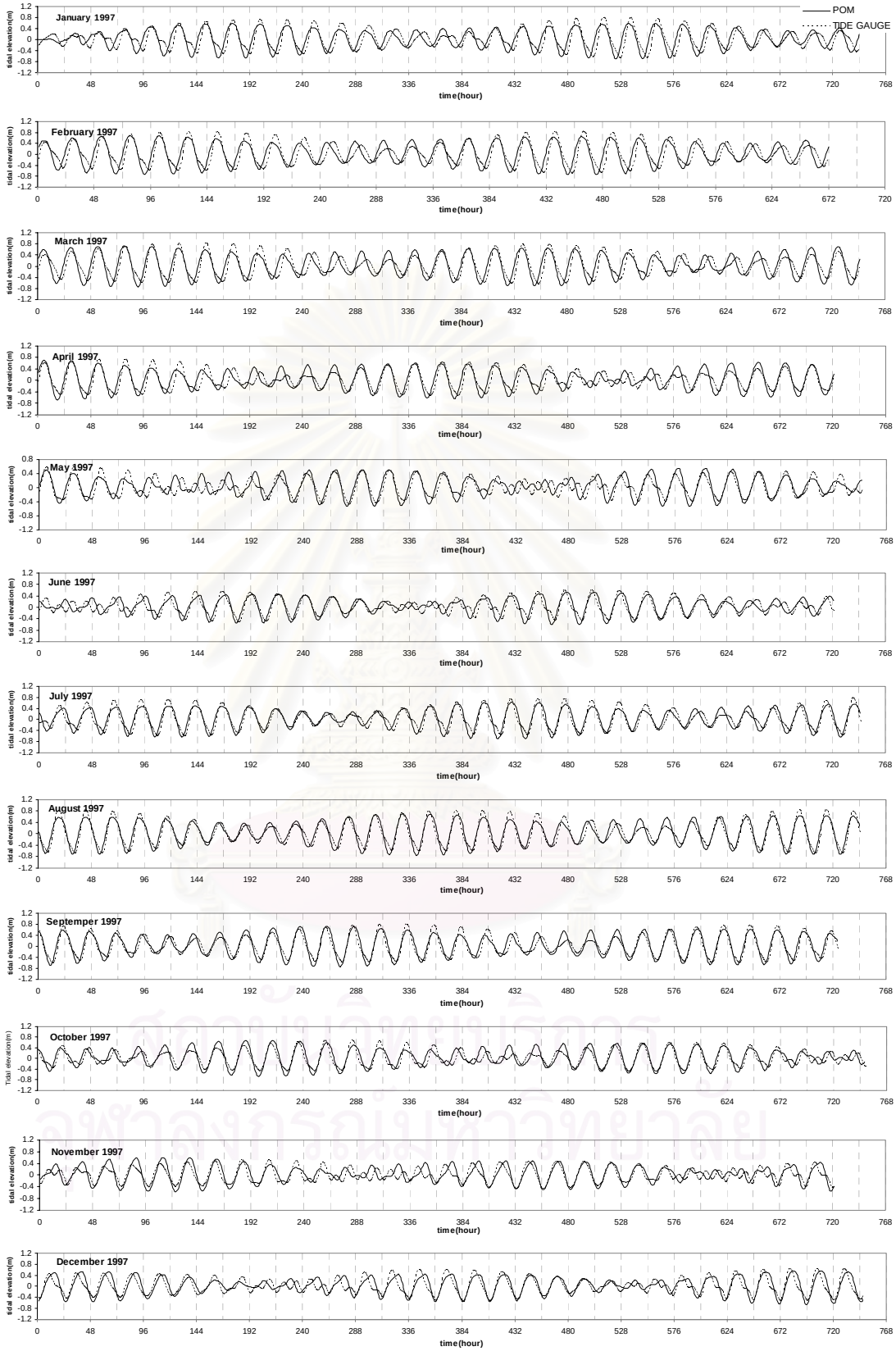

Figure 4.4(D) The comparison of the tidal elevation (in meters) between the hydrodynamic model based on POM and observed at Ko Mattapone station

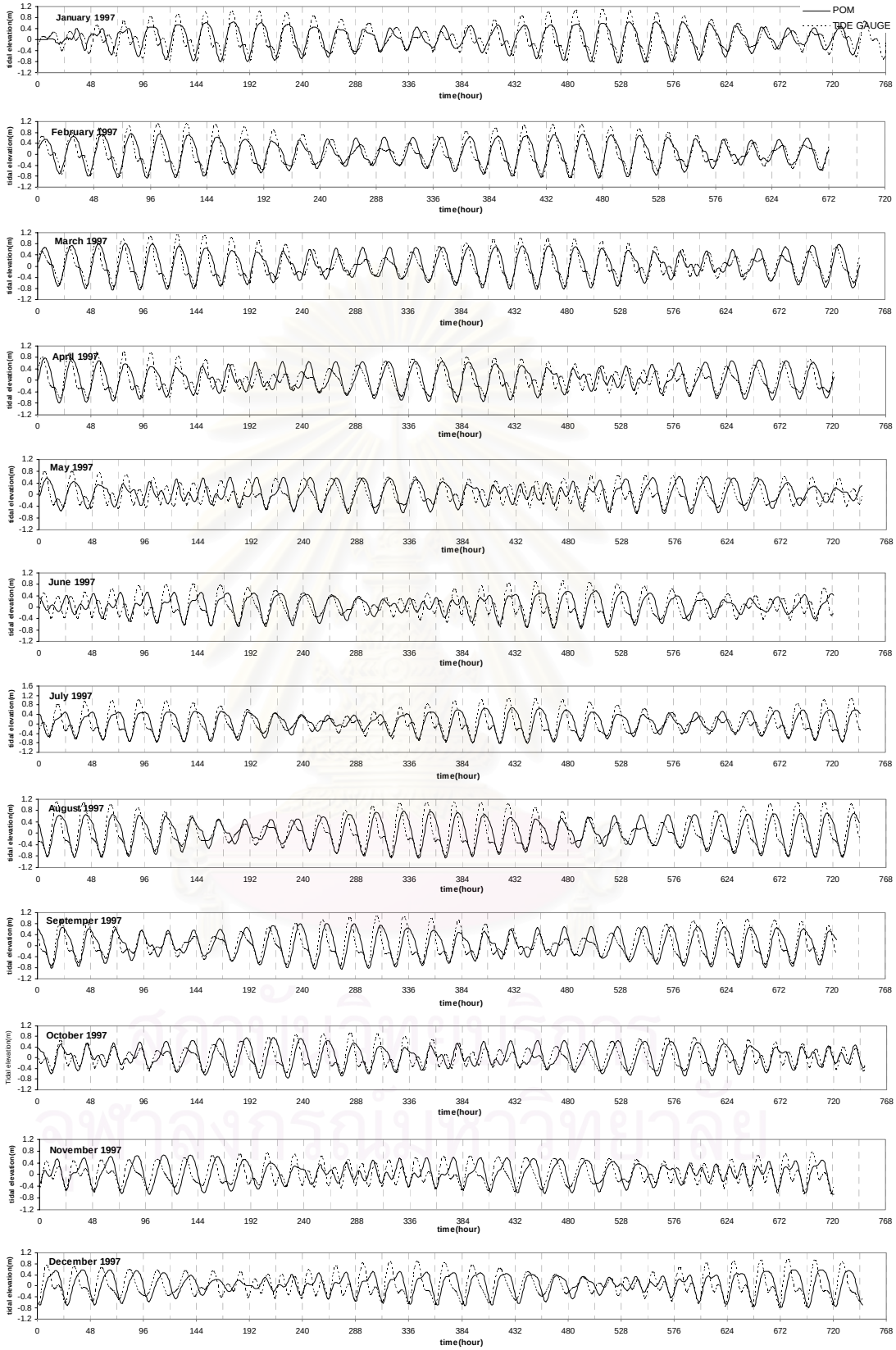

Figure 4.4(D) The comparison of the tidal elevation (in meters) between the hydrodynamic model based on POM and observed at Ko Prab station

Experiment II : Model response to a combination of meteorological forcing and co-oscillation tide

The interaction between tide and surge was carried out based on the occurrence of Typhoon Linda. The hydrodynamic model was executed covering the period from October 20, 1997 to November 9, 1997. Tide strongly affected the sea surface elevation. However, during strong wind condition (tropical storm), the sea surface elevation was also dominated by wind surge as depicted in Figure 4.5. Thus, it is necessary to combine the effect of tide and meteorological factors into the simulation of the sea surface elevation.

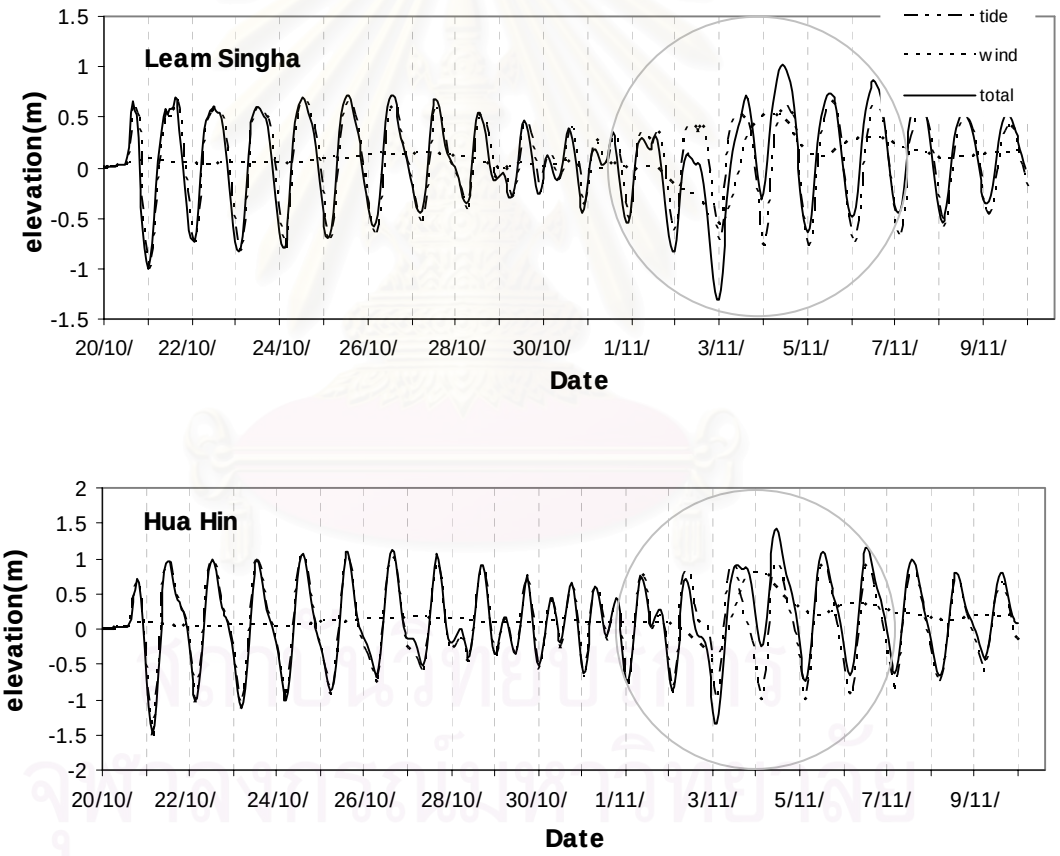

Figure 4.5 Temporal variation of the total water level from the hydrodynamic model based on POM for the period 20 October to 9 November 1997 at 5 tide gauge stations

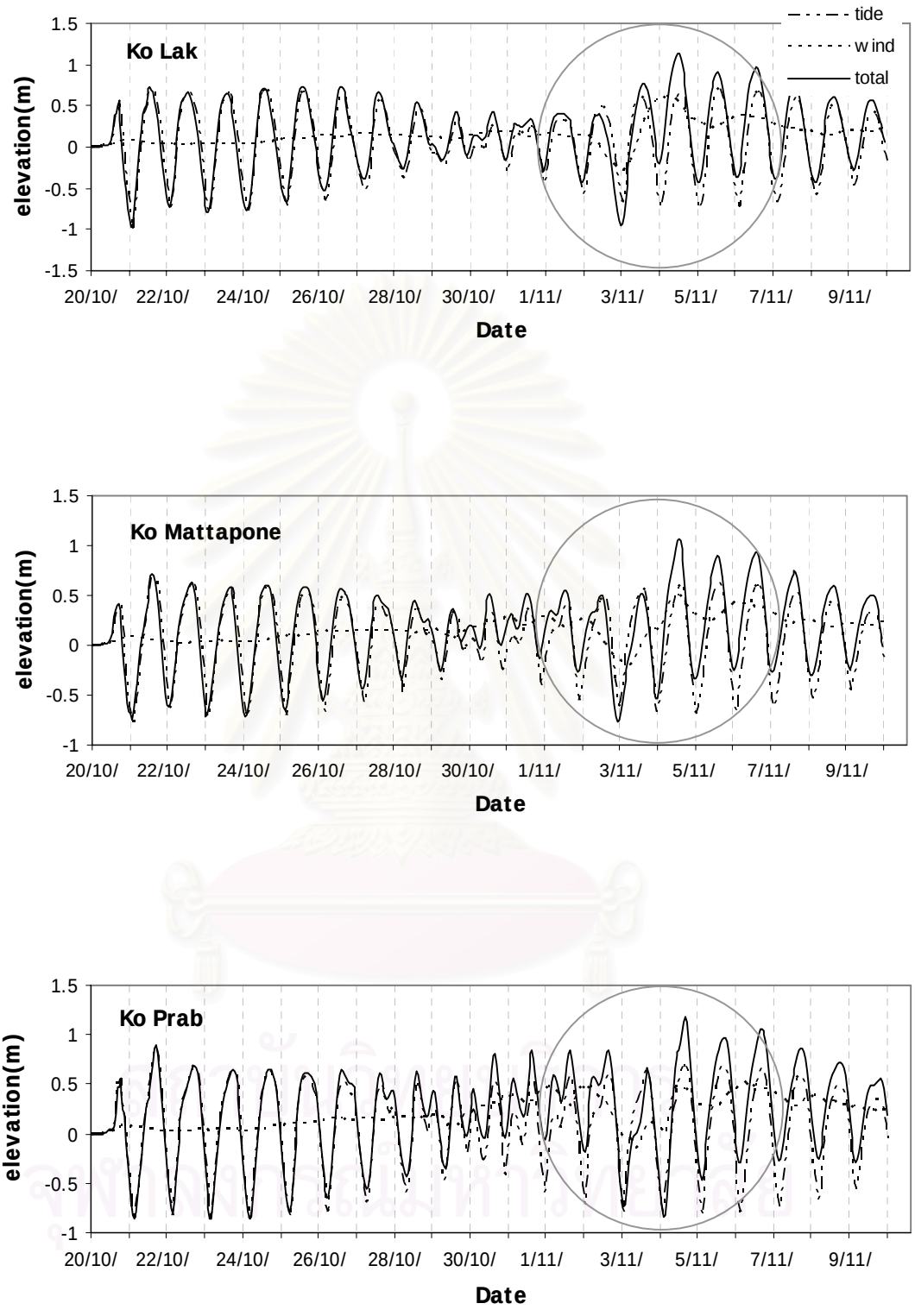

Figure 4.5 (continued) Temporal variation of the total water level from the hydrodynamic model based on POM for the period 20 October to 9 November 1997 at 5 tide gauge stations

The comparison of hourly time series sea surface elevation between the results from POM with different drag coefficients and the observed data at 4 tide gauges were shown in Figure 4.6(A) to 4.6(D). There were only four tide gauge data available during this period, namely Leam Singha, Ko Lak, Ko Mattapone, and Ko Prab. Sea surface elevation from POM and from tide gauges fluctuated in similar pattern. These plots showed that the surface elevation from POM correlated with the observed elevation at almost all stations, except at Ko Prab station. They showed a sudden drop of sea level as Linda entered the Gulf. Then, when Linda approached, there was a rapid rise of sea level to the highest point on 4th November at 12.00 am. After that, the sea level gradually dropped to normal fluctuation.

The results of sea surface elevations from each experiment were distinctive. At all stations, the model overestimated the sea surface elevation before the storm approached; in contrast, after the storm crossed over the Gulf, the model underestimated the sea surface elevation. During the storm surge, the peak sea surface elevation from POM was lower than the observed values as shown in Table 4.4(A). One reason is wind field which, for this study, is derived from global numerical weather prediction model with coarse resolution (1 degree), resulting in uniform wind field over the Inner Gulf. Moreover, the model only response to prescribed tide, wind and initial horizontal density gradient and stratification in the water column, other governing processes are not considered by this model such as fresh water discharge.

Before the storm approached, the sea surface elevation dropped to the lowest point. The predicted values differed from the observed values as listed in Table 4.4(B).

Table 4.4(A) The difference in the highest peak of sea surface elevation between the simulation and observation values

Experiment	The different of sea surface elevation (in m)			
	Leam Singha	Ko Lak	Ko Mattapone	Ko Prab
A	- 0.394	- 0.418	- 0.543	- 0.994
B	- 0.381	- 0.440	- 0.604	- 1.083
C	- 0.352	- 0.352	- 0.477	- 0.925
D	- 0.211	- 0.186	- 0.306	- 0.751

Table 4.4(B) The difference in the lowest peak of sea surface elevation between the simulation and observation values

Experiment	The different of sea surface elevation (in m)			
	Leam Singha	Ko Lak	Ko Mattapone	Ko Prab
A	0.08	0.02	0.06	-0.25
B	-0.03	-0.18	-0.19	-0.47
C	0.07	0.02	0.06	-0.24
D	-0.20	-0.02	0.05	-0.24

* Positive indicate the simulated values higher than the observed values

* Negative indicate the simulated lower than the observed values

Table 4.5 The Correlation coefficient (R^2) of each experiments

Experiment	Correlation coefficient (R)			
	Leam Singha	Ko Lak	Ko Mattapone	Ko Prab
A	0.84	0.83	0.79	0.63
B	0.84	0.84	0.84	0.73
C	0.83	0.84	0.80	0.64
D	0.84	0.84	0.83	0.64

In addition, the accuracy of a model for this purpose can be assessed by calculating the differences between the model and observed elevation and timing. The goodness-of-fit between the time series of the model and observed elevations can be described by the following reliability index, RI (Keen et.al.1998)

$$RI_i = \frac{1 + \sqrt{\frac{1}{T}\sum_{t=1}^{T}\left[\frac{1 - Y_{ti}/X_{ti}}{1 + Y_{ti}/X_{ti}}\right]^2}}{1 - \sqrt{\frac{1}{T}\sum_{t=1}^{T}\left[\frac{1 - Y_{ti}/X_{ti}}{1 + Y_{ti}/X_{ti}}\right]^2}}$$

where *i* is the mooring number; *T* is the total number of pairs of data points in the time series; Y_{ti} is the observation at mooring *i* for time t ; X_{ti} is the model result at the same location and time.

The model predictions are perfect if RI equal to 1 and no relationship when RI equal to 0.

Table 4.6 The Reliability Index of each experiment

Experiment	RI			
	Leam Singha	Ko Lak	Ko Mattapone	Ko Prab
A	1.11	1.10	1.10	1.17
B	1.13	1.14	1.12	1.20
C	1.11	1.10	1.10	1.16
D	1.11	1.10	1.10	1.16

In summary, the best correlation between POM results and the observed values was found in experiment D by considering the correlation coefficients (R^2) and Reliability Index (RI) (see Table 4.5 and 4.6). Therefore, C_D in experiment D was used to calculate wind stress in further study.

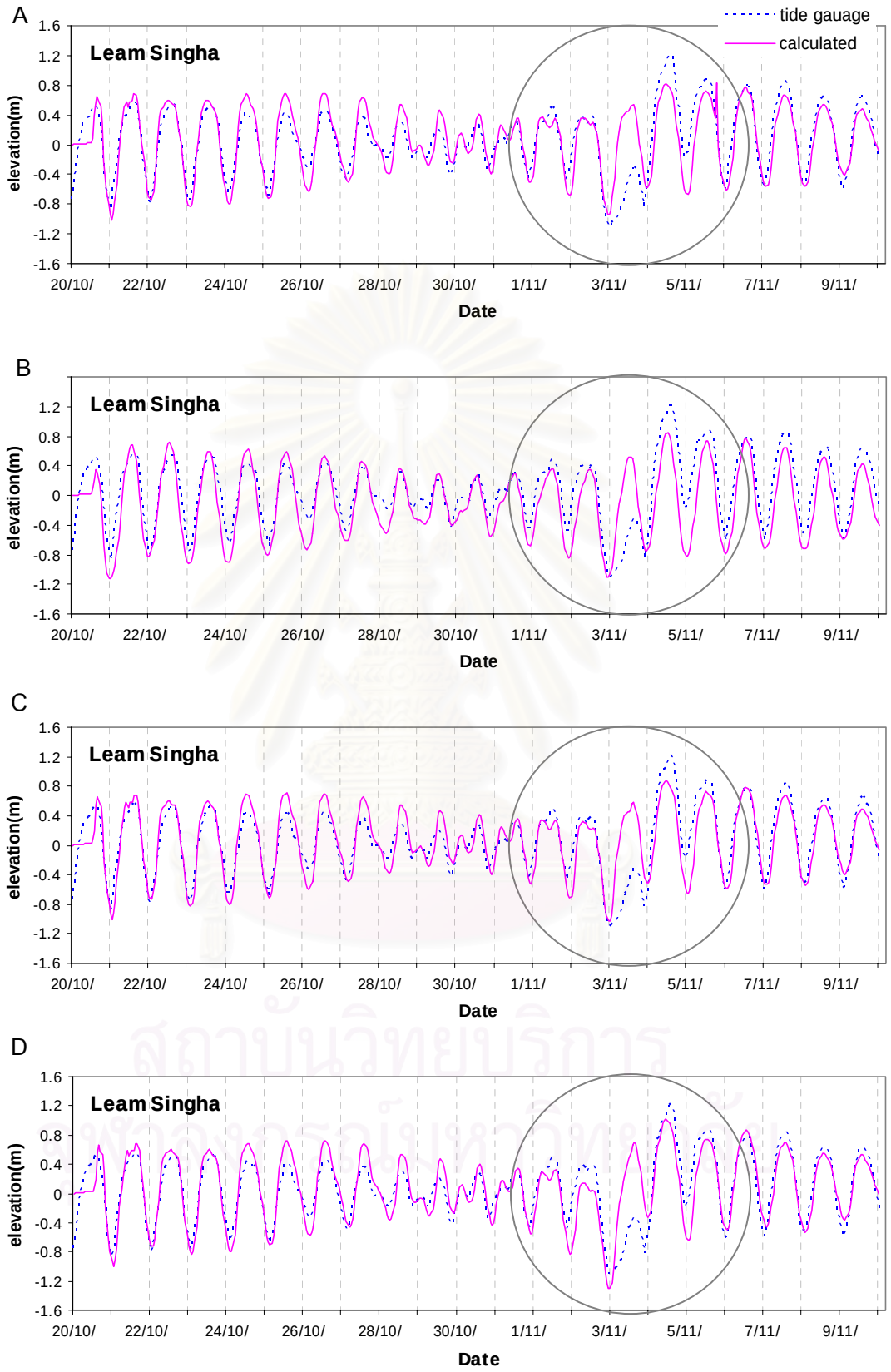

Figure 4.6(A) Temporal variation of sea surface elevation of experiment A, B, C, and D respectively. These plots covered the period from October 20 to November 9, 1997 at Leam Singha station

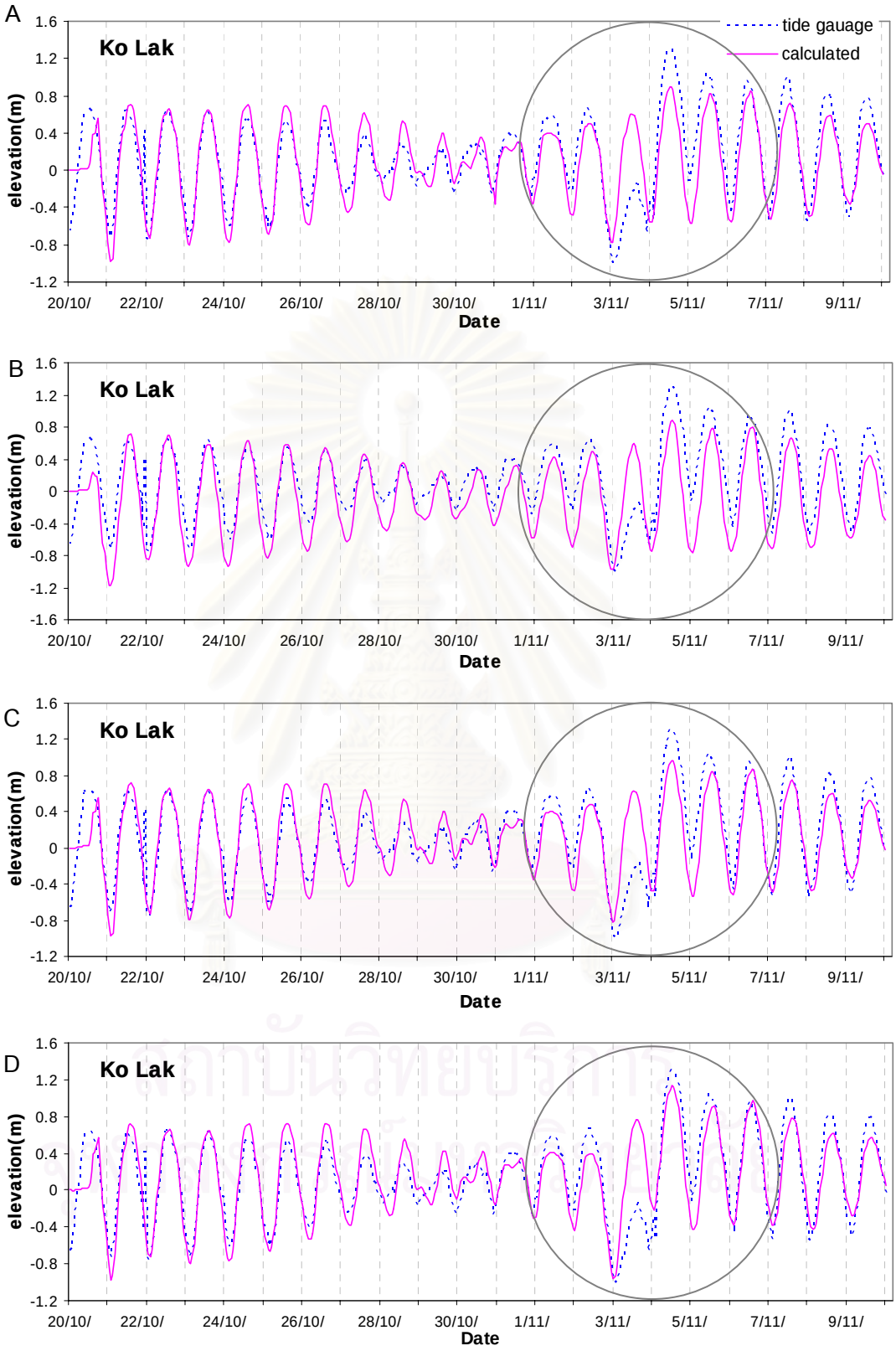

Figure 4.6(B) Temporal variation of sea surface elevation of experiment A, B, C, and D respectively. These plots covered the period from October 20 to November 9, 1997 at Ko Lak station

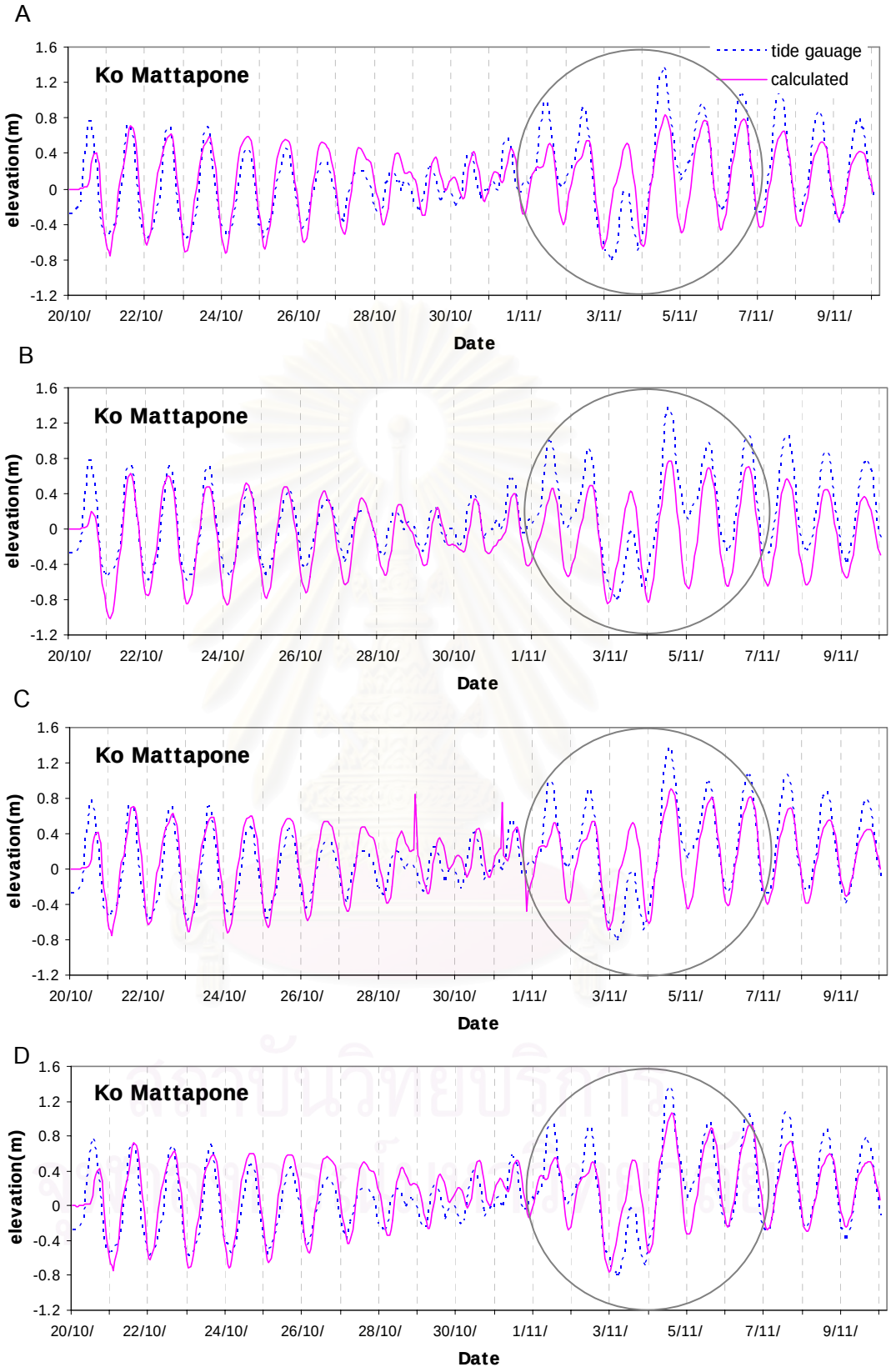

Figure 4.6(C) Temporal variation of sea surface elevation of experiment A, B, C, and D respectively. These plots covered the period from October 20 to November 9, 1997 at Ko Mattapone station

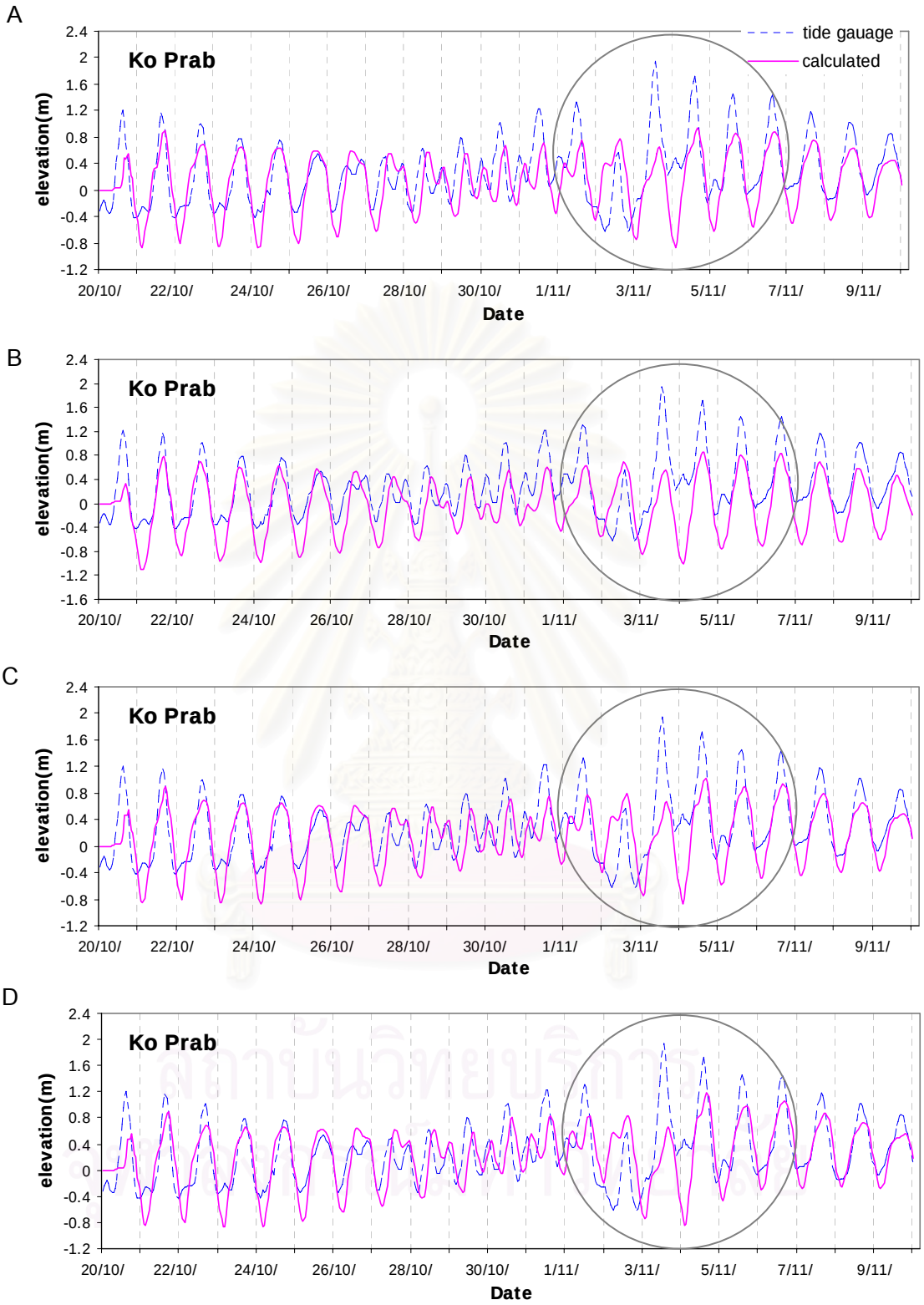

Figure 4.6(D) Temporal variation of sea surface elevation of experiment A, B, C, and D respectively. These plots covered the period from October 20 to November 9, 1997 at Ko Prab station

The wind stress and simulated currents from the model was illustrated in Figure 4.7 (selected scenes). The strong current, produced by strong wind, flowed from the South China Sea into the Gulf of Thailand. The circulation from the model agreed well with the best track data of Typhoon Linda as illustrated in Figure F.1 (in appendix E). Unfortunately, there were no observation data to verify the model results.

From the variation in currents and sea surface elevations, it can be divided into 3 stages: before the passage of storm surge, the existing of storm surge and after the passage of surge.

The first stage (before the passage of storm surge), in general, the current in the Gulf were dominated by tide (see Figure 4.7(A) and (B)). The currents flowed out from the inner of the Gulf (ebb) into South China Sea; in simultaneously, the strong current flowed northwestward from South China Sea into the Gulf. It was divided the circulation into two parts at the South of Cape Camau of Vietnam, one moved westward into the southeastern part of the Gulf of Thailand along the coast of Cambodia and Vietnam, and the other moved southward along the coast of Malaysia. Twelve hours later, the currents flowed northward along the eastern and western of the Gulf into the Gulf (flood).

The second stage (during the occurring of storm surge), the developing of typhoon Linda starting on 2 November 1997 at 000 UTC to 4 November 1997 is depicted in Figure 4.7(C) to (G). On 2 November 1997 at 000 UTC, the typhoon wind was located at latitude 8.2 N and longitude 107.6 E. Its central pressure and maximum wind speed are 995 millibars and 45 konts respectively. Then, it moved northeastward to Cape Camau of Vietnam in twelve hours later. After that, it moved in the same direction into the Gulf, and hit the coast at Thupsake, Changwat Prachupkirikhun at 0.00 on 4 November 1997. These figures showed that the strong current from South China Sea flowed northwestward into the Gulf, and turned to the north along the eastern part of the Gulf. After that, it turned to the southern part of the Gulf. As a result, a counter-clockwise circulation was presented at southern part of the Gulf.

The final stage (after the passage of surge), the currents decreased in strength but the counter-clockwise circulation existed in the same location. The currents from the upper Gulf moved southward along the eastern part of the Gulf and the coast of Vietnam and Cambodia into South China Sea (Figure 4.7(H)).

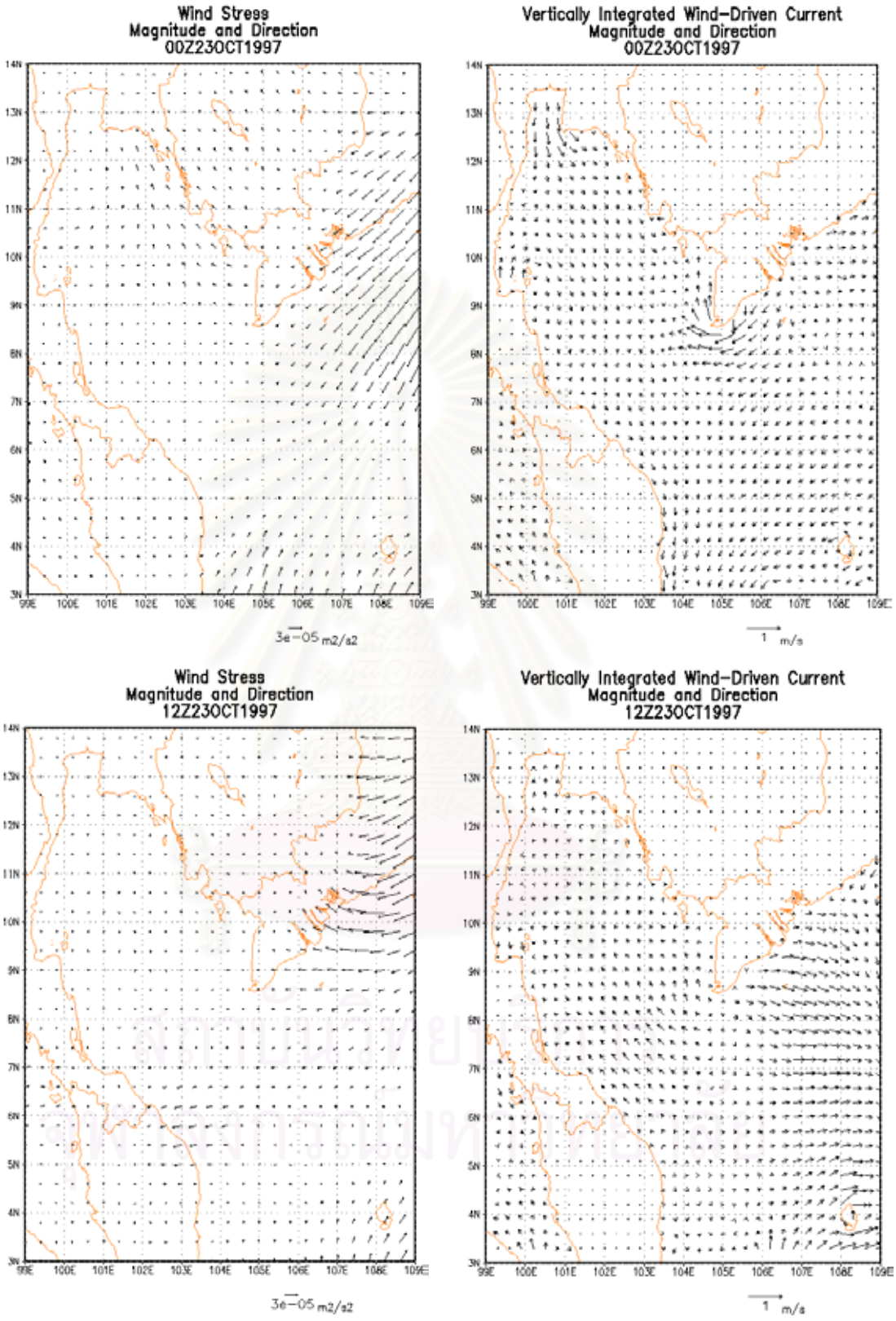

Figure 4.7 The Simulated currents (A) October 23, 1997 at 00:00 (B) October 23, 1997 at 12:00

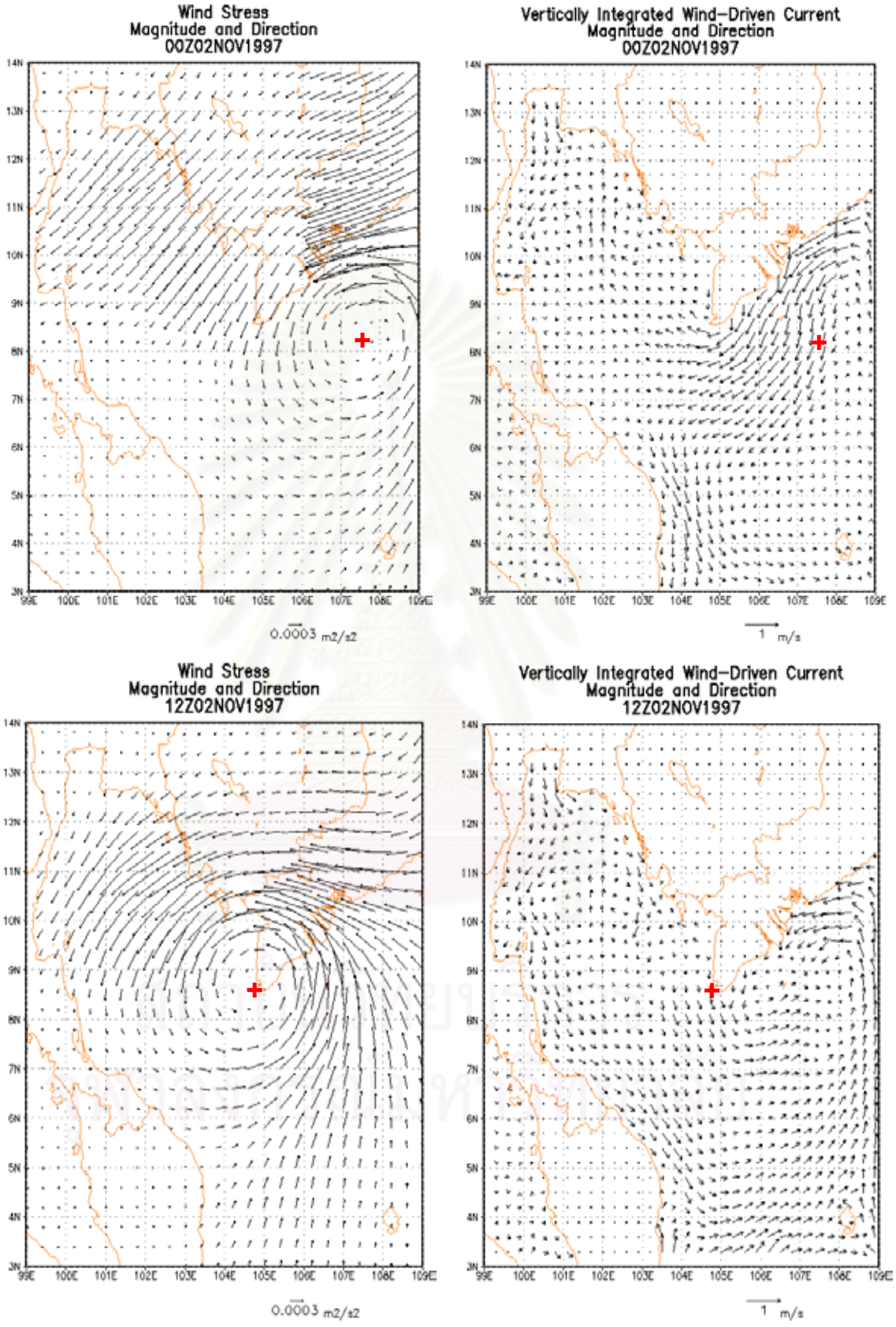

Figure 4.7 The Simulated currents (C) November 02, 1997 at 00:00 (D) November 02, 1997 at 12:00

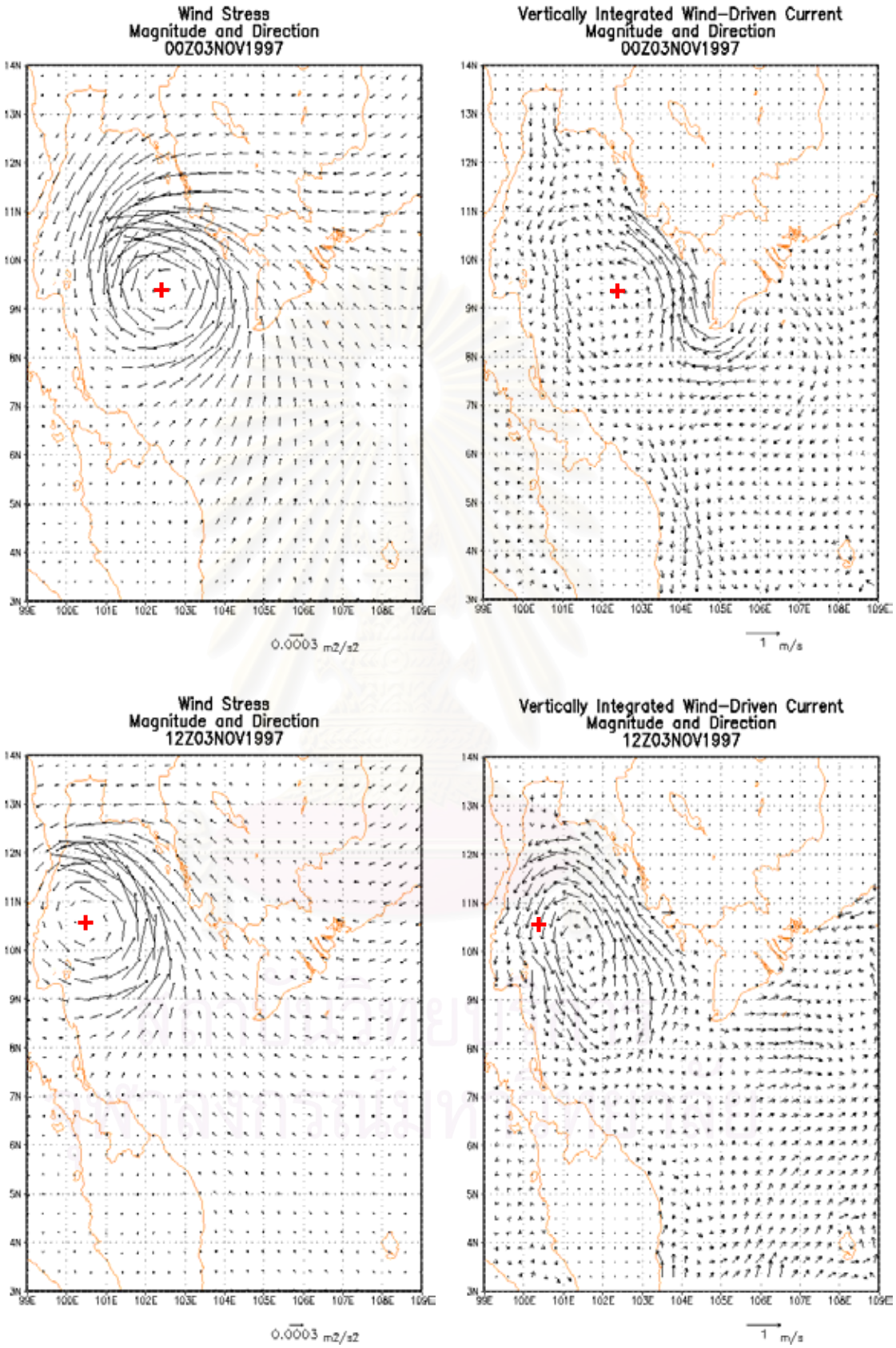

Figure 4.7 The Simulated currents (E) November 03, 1997 at 00:00 (F) November 03, 1997 at 12:00

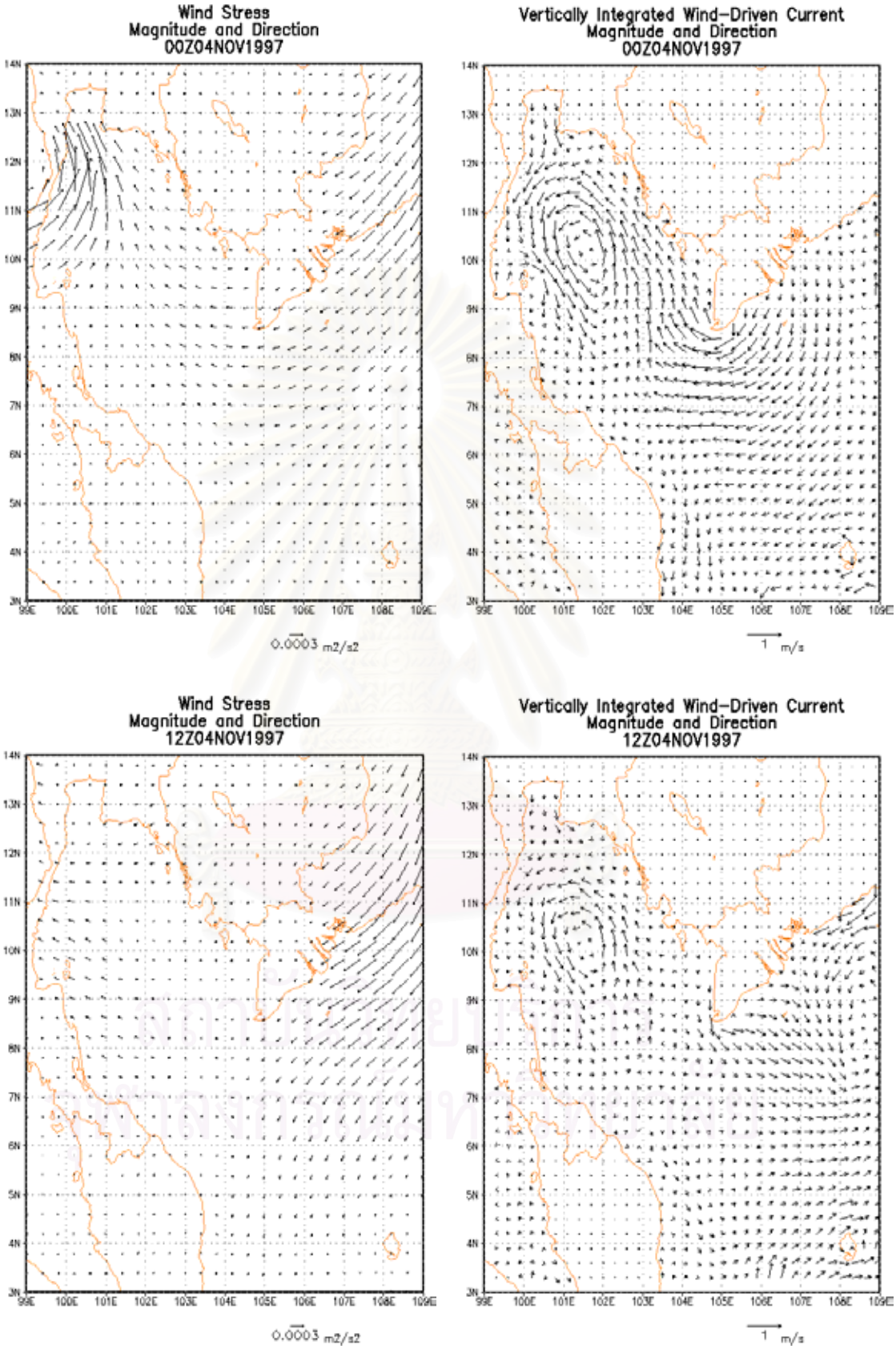

Figure 4.7 The Simulated currents (G) November 04, 1997 at 00:00 (H) November 04, 1997 at 12:00

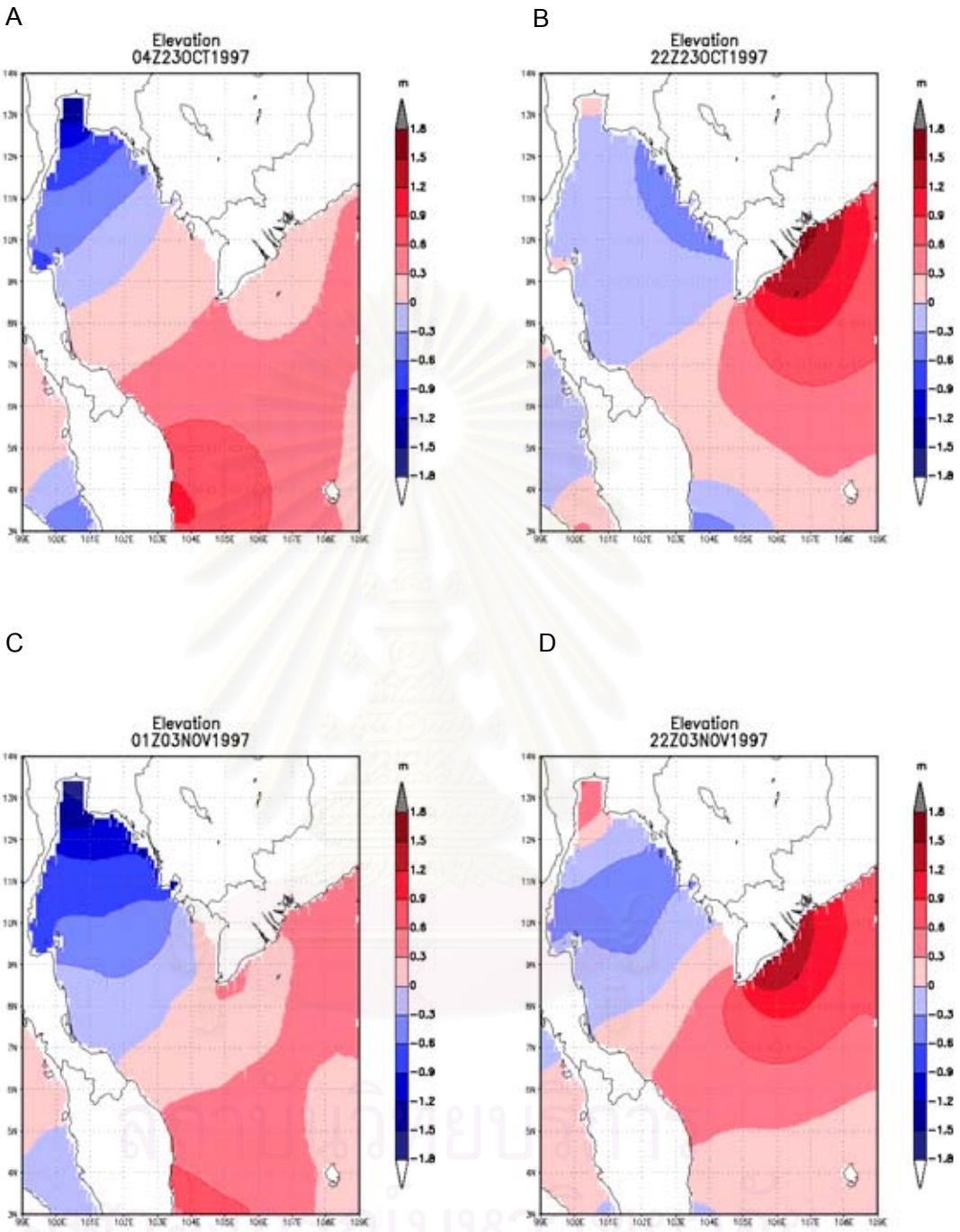

Figure 4.8 Simulated sea surface elevation (A) October 23,1997 04:00 (B) October 23,1997 22:00 (C) November 3,1997 01:00 (D) November 3,1997 22:00

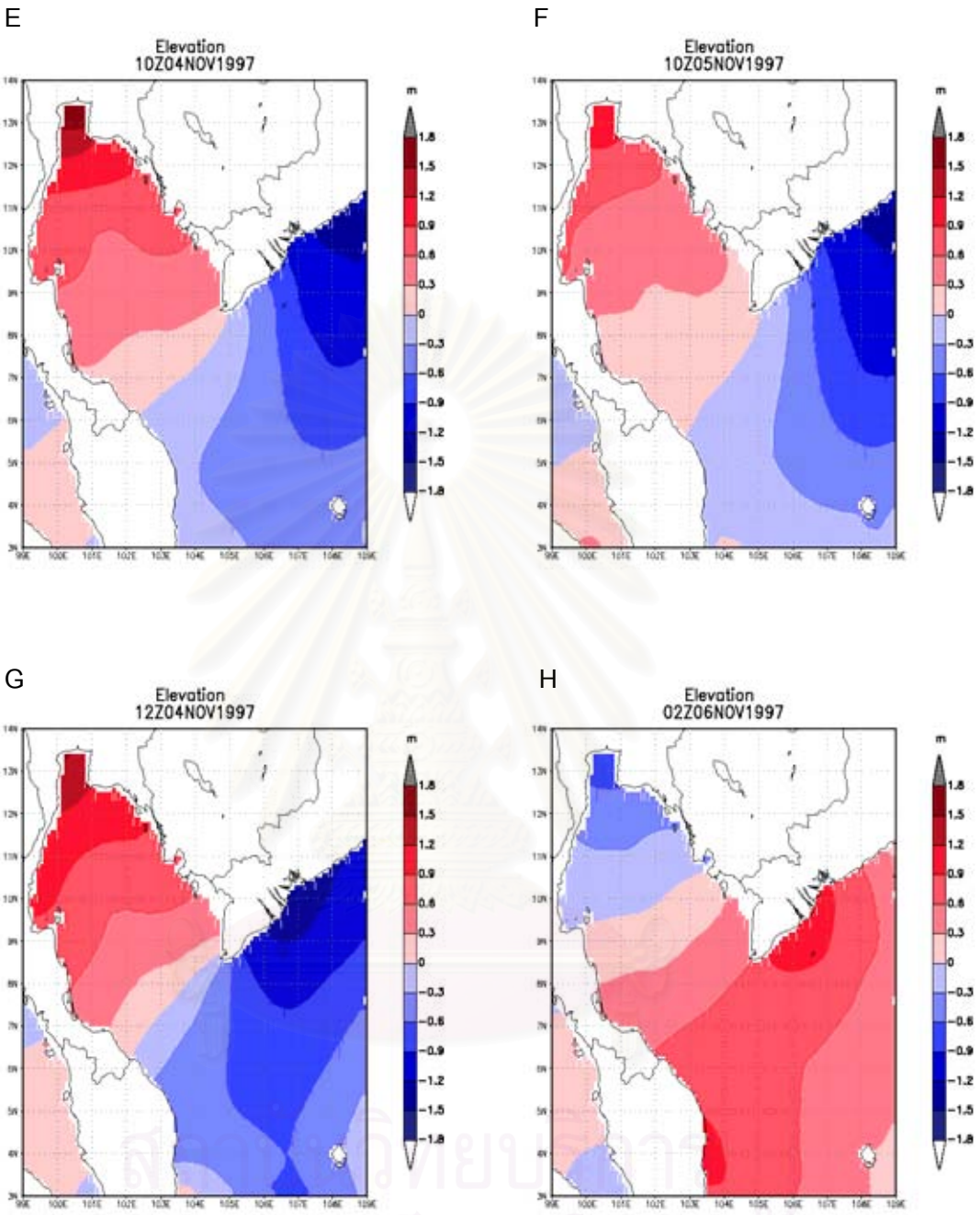

Figure 4.8 (continued) Simulated sea surface elevation (E) November 4,1997 10:00 (F) November 4,1997 12:00 (G) November 5,1997 10:00 (H) November 6,1997 02:00

The simulated sea surface elevations from the model were shown in Figure 4.8(A) to (D). Before the occurring the storm, sea surface elevation fluctuated with tide (Figure 4.8(A) and (B)). Before the surge hit the land, the entire sea surface elevation decreased to the lowest point, and then the sea surface elevations sharply rose to the highest peak as the storm entered the Gulf (see Figure 4.8 (C) to (G)). After that, the sea level gradually decreases to normal fluctuation. The storm strongly affected on the sea surface elevation especially in the upper part of the Gulf (upper of the track) due to the shape of this area.

Experiment III : Model verification with other storms

The hindcast simulation of sea surface elevation in case of typhoon Linda showed that the simulated sea surface levels corresponded well with the observed ones. Therefore, in this section, the above model was applied to investigate the storm surge caused by the low pressure that crossed over the Gulf of Thailand, namely Chip and Gil in 1998. Figure 4.9 to 4.10 showed that the model can depict the temporal variation of sea surface elevation disturbed by the strong wind.

The sea surface elevations from the model were in good agreement with the observations at most of the tide gauges. The sea surface elevations obtained from POM were about 10 cm less than the observed values since the observed values composed of more than one hundred constituents while the model results had only eight constituents. Additionally, the northeast wind can push water into the Gulf but the model did not account for this because the wind fields derived from global numerical weather prediction model had coarse resolution (1 degree) resulting in uniform wind field over the Upper Gulf of Thailand and were less than the actual wind velocities. However, the model accurately generated sea surface fluctuation though at some points the fluctuation was not in phase with the observed tide.

In summary, the results showed that the accuracy in the simulated currents and sea surface elevations depends on various factors: the shape and depth of model domain, the accuracy of the prescribed tide at the defined open boundaries, the river

runoff from heavy rainfall which accompanied with storm wind, and wind fields as input forcing functions.

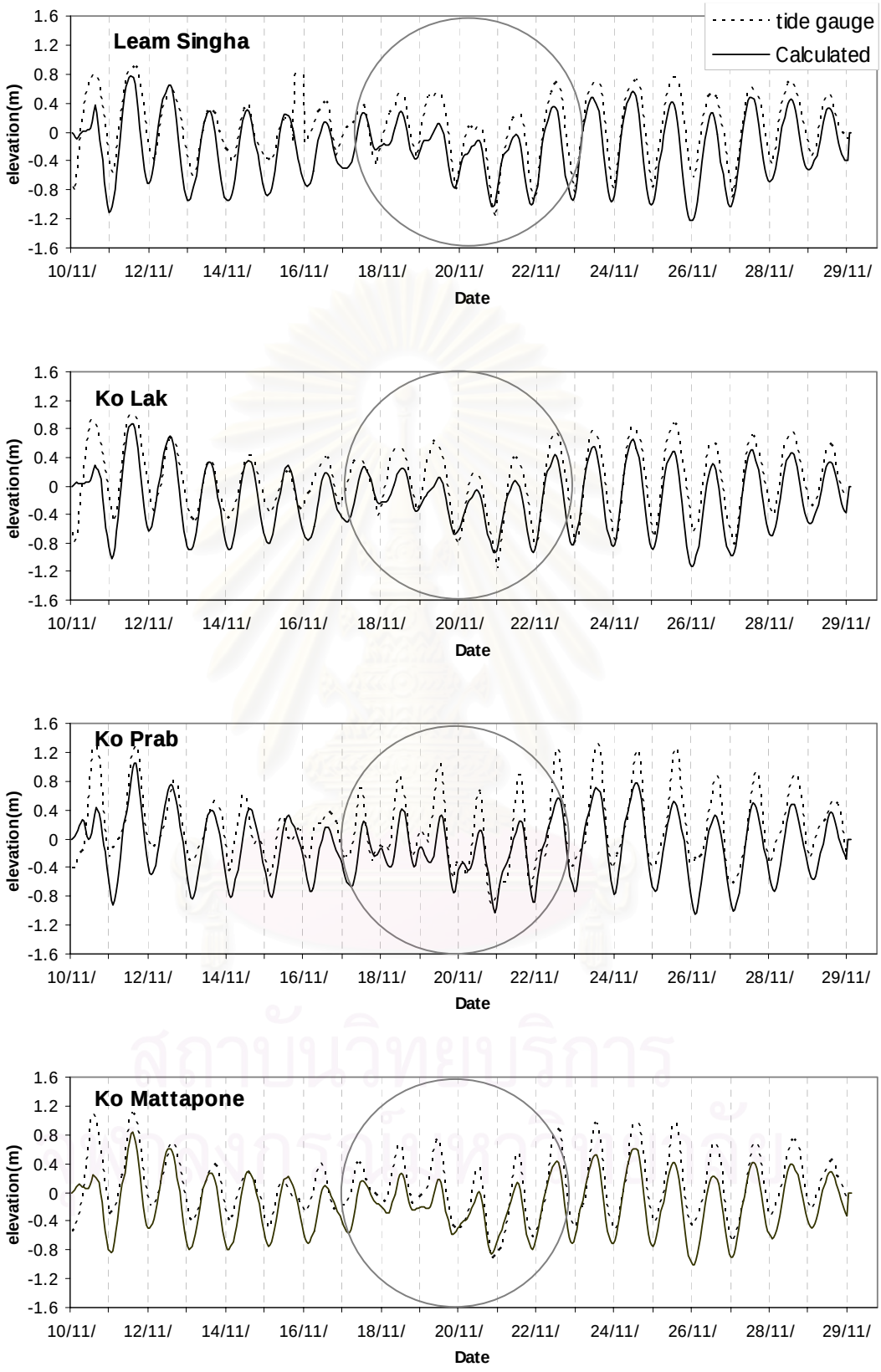

Figure 4.9 Comparison of hourly time series sea surface elevation at 4 stations covering the period from November 10 to 30, 1998 (Chip)

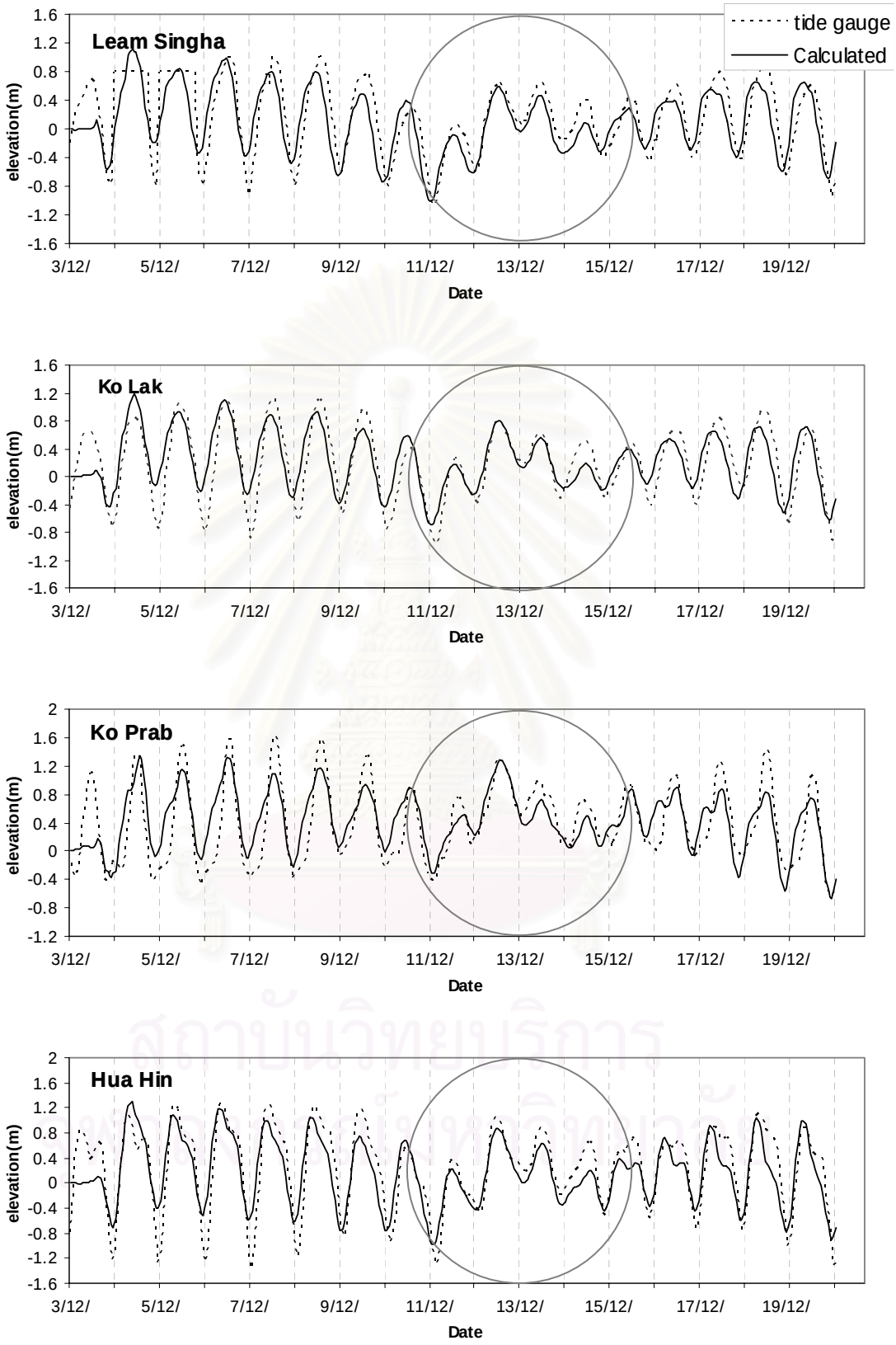

Figure 4.10 Comparison of hourly time series sea surface elevation at 4 stations covering the period from December 9 to December 20, 1998 (Gil)

CHAPTER 5

CONCLUSIONS

In this study, POM was modified and applied to investigate the effect of typhoon Linda on the sea surface elevation in the Gulf of Thailand. The model was driven by the combination of wind stress from numerical weather prediction (12 hourly), co-oscillation tide in terms of harmonic constants at open boundaries and initial climatological horizontal density gradient and stratification during the period from October 20, 1997 to November 9, 1997. The model was then used to verify with other storms, namely Chip and Gil during the period from November 10 to 30, 1998 and December 9 to 20, 1998 respectively.

The use of numerical experiments indicates that tide is the essential factor to simulate the sea surface elevation in the Gulf of Thailand. However, interaction between tide and wind account for sea level rise during storm surge period. POM can effectively simulate sea surface elevation disturbed by storm-surge in case of low pressure wind intensity (Chip and Gil). The model accurately generated sea surface fluctuation although at some points, the fluctuation was not in phase with the observed tide. In case of strong wind (typhoon Linda), the maximum predicted water levels were less than observed maximum surge due to various reasons. The first reason is that lower wind fields and atmospheric pressure and coarse resolution were used in this study. Second, the coarse and inaccuracy bathymetry for model simulations can cause the discrepancy in sea surface elevation between the model results and observed ones. For instance, Ko Prab located behind Ko Samui and Ko Pha-Ngan but the model do not account for the presence of island at Ko Samui. Finally, the other governing processes such as fresh water discharge which are not considered by this model can cause the discrepancy in sea surface elevation.

There are many issues that remain to be resolved in order to improve model performance. Wind field is an essential factor affecting the sea surface elevation

especially in the period of storm. The better accuracy and spatial resolution of local numerical weather prediction data are needed for the model simulation. The accuracy of model results can improve in various ways as described below:

- The model responses to co-oscillation tide of only eight principal constituents (M_2, S_2, K_1, O_1, P_1, Q_1, N_2, and K_2). Inclusion of other constituents such as S_a in the Gulf of Thailand may improve the model accuracy.

- The effect of the freshwater discharged into the Gulf should be considered especially at estuary or river mouth.

Recently, the numerical model has become a powerful tool for various fields of sciences. It can be used in many ways such as warning system, prediction, and monitoring. However, adequate observed data are the most important information to improve the accuracy of the model.

References

Andersen, B. 1998. Shallow water tides in the northwest European shelf region from TOPEX/POSEIDON altimetry. Journal of geophysical research 104: 7729-7741.

Bowden, K.F. 1983. Physical Oceanography pf Coastal Waters. Southampton: Ellis Horwood. 302 pp.

Buranaprattheprat, A. 2003. Seasonal Variations in Circulation and Average Residence Time of the Bangpakong Estuary, Thailand. In The First Joint Seminar on Coastal Oceanography: Program and Abstracts. 14-16 December 2003 Chiang Mai, Thailand. Japanese Society for the Promotion of Science National Research Council of Thailand.

Chapman, M.D. 1994. Natural Hazards. Melbourne: Oxford University Press, 174 pp.

Chu, C.P., Lu, S. and Chen, Y. 2001. Evaluation of the Princeton Ocean Model Using South China Sea Monsoon Experiment (SCSMEX) Data. Journal of Atmospheric and Oceanic Technology 18:1521-1539.

Cowden, D.J.; Croxton, F.E.; and Klein S. 1969. applied general statistics. 3 nd ed. India: Prince Hall

Flather, A.R. 1994. A Storm Surge Prediction Model for the Northern Bay of Bengal with Application to the Cyclone Disaster in April 1991. Journal of Physical Oceanography 24: 172-190.

Groves, D. 1989. The Oceans. John Wiley & Sons, 203 pp.

Humphreys, W.J. 1964. Physics of the Air. New York: Dover Publication, 676 pp.

Johnston, M.D. 1998. Seapol Integrated Studies of the Gulf of Thailand Volume 1. Southeast Asian Programme in Ocean Law, Policy and Management. Bangkok: Innomedia.

Joint Typhoon Warning Center. SUMMARY OF WESTERN NORTH PACIFIC AND NORTH INDIAN OCEAN TROPICAL CYCLONES [Online]. Available from: https://metoc.npmoc.navy.mil/jtwc/atcr/1997atcr/ch3/30w.htm[2004, January23]

Keen, R.T. and Glenn, S.M. 1998. Factors Influencing Modeling Skill for Hindcasting Shallow Water Currents during Hurricane Andrew. Journal of Atmospheric and Oceanic Technology 15: 221-236.

Lekphliphol, S. 1998. Tropical storm in the Gulf of Thailand in the last 10 year. The effects of Typhoon Linda in the Gulf of Thailand and the coastal area conference, 5 June 1998, Bangkok. Chulalongkorn University.

Mellor, G.L. 2002. User guide for a three-dimensional primitive equation numerical ocean model. New Jersey: Program in Atmospheric and Oceanic Sciences, Princeton University. [Online].
Available from http://www.aos.princeton.edu/WWWPUBLIC/htdocs.pom/ [2002,July]

Morimoto, A. Yoshimoto, K. and Yanagi, T. 2000. Characteristics of Sea Surface Circulation and Eddy Field in the South China Sea Revealed by Satellite Altimetric Data. Journal of Oceanography 56:331-344.

Morimoto, A. and Matsuda, T. 2003. Satellite Altimetry Data Set in the Asian Marginal Seas. In The First Joint Seminar on Coastal Oceanography: Program and Abstracts. 14-16 December 2003 Chiang Mai, Thailand. Japanese Society for the Promotion of Science National Research Council of Thailand.

Oopan, S. 2003. Effects of tide and wind on simulated current in the Gulf of Thailand. A Thesis submitted in partial fulfillment of the requirements for the degree of Master of Science. Chulalongkorn University.

Pal, B.K. and Holloway, G. 1996. Dynamics of circulation off the west coast of Vancouver Island. Continental Shelf Research 16(12):1591-1607.

Pond, S. and Pickard, L.G. 1983. Introductory Dynamical Oceanography, 2nd ed. New York: Pergamon Press, 329 pp.

Pugh, T.D. 1987. Tides, Surges and Mean Sea – Level. London: John Wiley & Sons, 472 pp.

Schjolberg, P. 1998. Preliminary results from an ocean circulation model for the Gulf of Thailand during Linda. The effects of Typhoon Linda in the Gulf of Thailand and the coastal area conference, 5 June 1998, Bangkok. Chulalongkorn University.

Smith, K. 1996. Environmental Hazards 2nd edition Assessing risk and reducing disaster. London: Routledge. 389 pp.

Snidvong, A. 2003. Eye on the Ocean: Bringing the Sea to the Classroom. Bangkok.

Tang, M.Y., Grimsham, R., Sanderson, B. and Holland, G. 1996. A numerical study of Storm Surge and Tides with Application to the North Queensland Coast. Journal of Physical Oceanography 26:2700-2711.

Tang, M.Y., Holloway, P. and Grimshew, R. 1997. A Numerical Study of the Storm Surge Generated by Tropical Cyclone Jane. Journal of Physical Oceanography 27: 963-976.

Thai Meteorological Department. The information of Meteorology [Online]. Available from: www.tmd.go.th [2004, March14]

Wangwongchai, A. 1998. Storm Surge Modeling over the Gulf of Thailand. A Thesis submitted in partial fulfillment of the requirements for the degree of Master of Science. King Mongkut's University of Technology Thonburi.

Wu, K.J, Xie, L.A. and Pietrafesa, L. J. 2002. A Numerical Study of Wave-Current Interaction through Surface and Bottom Stresses: Coastal Ocean Response to Hurricane Fran of 1996. In Proceedings The Seventh Workshop Ocean Models for the APEC Region (WOM-7).30 September – 2 October 2002,Singapore.

Tropical Marine Science Institute, The National University of Singapore. pp11.1-11.8.

Yanagi, T. and Takao, T. 1997. Clockwise Phase Propagation of Semi-Diurnal Tides in the Gulf of Thailand. Journal of Oceanography 54:143–150.

Ye, A.L. and Robinson, I.S. 1983. Tidal dynamics in the South China Sea. Geophys. J.R. asir. Soc. 72:691-707.

Zecchetto, S., Umgiesser, G. and Brocchini, M. 1997. Hindcast of a storm surge induced by local real wind fields in the Venice Lagoon. Continental shelf Research 17(12):1513 – 1538.

Zhang, M.Y. and Li, Y.S. 1996. The synchronous coupling of a third-generation wave model and two-dimensional storm surge model. Ocean Engng 23(6):533-543.

APPENDIXES

APPENDIX A

International Equation of State of Sea Water, 1980

The new equation of state is presented by Millero and Poisson (1981, cited in Pond and Pickard, 1983) and given in UNESCO Technical Paper in Marine Science Number 36 (UNESCO, 1981). The density of sea water (in kg m^{-3}) as a function of temperature T (^{o}C) range from -2 ^{o}C to 30 ^{o}C , salinity S (psu) from 20 to 40 psu , and pressure p (bars) from 0 to 1000 bars over the typical oceanic is given by

$$\rho(T,S,p) = \rho(T,S,0)[1 - p/K(T,S,p)]^{-1} \qquad \text{(A.1)}$$

where $K(T,S,p)$ is the secant bulk modulus. The polynomial expressions for $\rho(T,S,0)$ and $K(T,S,p)$ are given below.

For the IES 80, the density of sea water at one standard atmosphere pressure $(p = 0)$ is given by:

$\rho(T,S,0)$ =

$$\begin{aligned}
&+ 999.842\,594 && + 6.793\,952 \times 10^{-2}\, T \\
&- 9.095\,290 \times 10^{-3}\, T^2 && + 1.001\,685 \times 10^{-4}\, T^3 \\
&- 1.120\,083 \times 10^{-6}\, T^4 && + 6.536\,332 \times 10^{-9}\, T^5 \\
&+ 8.244\,93 \times 10^{-1}\, S && - 4.089\,9 \times 10^{-3}\, TS \\
&+ 7.643\,80 \times 10^{-5}\, T^2S && - 8.246\,7 \times 10^{-7}\, T^3S \\
&+ 5.387\,50 \times 10^{-9}\, T^4S && - 5.724\,66 \times 10^{-3}\, S^{1.5} \\
&+ 1.022\,70 \times 10^{-4}\, TS^{1.5} && - 1.654\,6 \times 10^{-6}\, T^2S^{1.5} \\
&+ 4.831\,40 \times 10^{-4}\, S^2 && \qquad \text{(A.2)}
\end{aligned}$$

For the IES 80, the secant bulk modulus is given by:

$$K(T,S,p) =$$

$$
\begin{aligned}
&+ 19\,652.21 \\
&+ 148.420\,6 && T && - 2.327\,105 && T^2 \\
&+ 1.360\,477 \times 10^{-2} && T^3 && - 5.155\,288 \times 10^{-5} && T^4 \\
&+ 3.239\,908 && p && + 1.437\,13 \times 10^{-3} && Tp \\
&+ 1.160\,92 \times 10^{-4} && T^2 p && - 5.779\,05 \times 10^{-7} && T^3 p \\
&+ 8.509\,35 \times 10^{-5} && p^2 && - 6.122\,93 \times 10^{-6} && Tp^2 \\
&+ 5.278\,7 \times 10^{-8} && T^2 p^2 \\
&+ 54.674\,6 && S && - 0.603\,459 && TS \\
&+ 1.099\,87 \times 10^{-2} && T^2 S && - 6.167\,0 \times 10^{-5} && T^3 S \\
&+ 7.944 \times 10^{-2} && S^{1.5} && + 1.648\,3 \times 10^{-2} && TS^{1.5} \\
&- 5.300\,9 \times 10^{-4} && T^2 S^{1.5} && + 2.283\,8 \times 10^{-3} && pS \\
&- 1.098\,1 \times 10^{-5} && TpS && - 1.607\,8 \times 10^{-6} && T^2 pS \\
&+ 1.910\,75 \times 10^{-4} && pS^{1.5} && - 9.934\,8 \times 10^{-7} && p^2 S \\
&+ 2.081\,6 \times 10\text{-}8 && Tp^2 S && + 9.169\,7 \times 10^{-10} && T^2 p^2 S
\end{aligned}
$$

(A.3)

The above polynomials are taken from UNESCO Technical Papers in Marine Science No. 36, 1981.

APPENDIX B

Arakawa C-grid

The straggered grid arrangement for external and internal mode is illustrated in **Figure B.1 to B.2** respectively (Mellor, 2002).

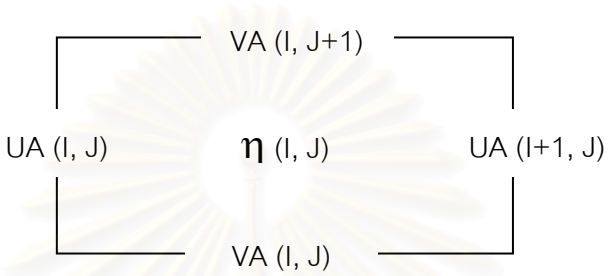

Figure B.1 The two-dimensional external mode grid

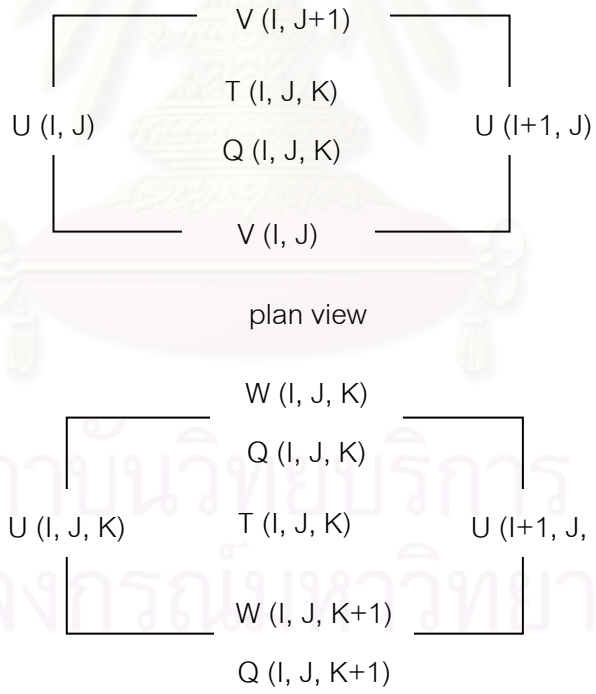

Figure B.2 The three- dimensional internal mode grid. Q represents km, kh, q2, or q2l, and T denotes as t, s, or rho.

APPENDIX C

TIME STEP CONSTRAINTS

The Courant-Friedrichs-Levy (CFL) computational stability condition on the external and internal mode as described below:

$$\Delta t_E \le \frac{1}{C_t}\left|\frac{1}{\delta x^2}+\frac{1}{\delta y^2}\right|^{-1/2} \tag{C.1}$$

$$\Delta t_i \le \frac{1}{C_T}\left|\frac{1}{\delta x^2}+\frac{1}{\delta y^2}\right|^{-1/2} \tag{C.2}$$

$$C_t = 2(gH)^{1/2} + U1_{\max} \tag{C.3}$$

$$C_T = 2C + U2_{\max} \tag{C.4}$$

where Δt_E and Δt_i are the limited time step for internal and external mode respectively. $U1_{\max}$ and $U2_{\max}$ are denoted as the expected maximum velocity and the maximum advective speed respectively. δx and δy are the grid spacing in x- and y- direction respectively.

APPENDIX D

Location of tide gauge stations and oceanographic buoys

No.	Station	Latitude (° N)	Longitude (° E)	observed data
1	Klong Yai	11.78	102.87	tidal elevation
2	Leam Ngob	12.10	102.40	tidal elevation
3	Laem Sing	12.47	102.07	tidal elevation
4	Prasae	12.7	101.70	tidal elevation
5	Rayong	12.67	101.28	tidal elevation
6	Ao Sattahip	12.65	100.88	tidal elevation
7	Ko Si Chang	13.15	100.82	tidal elevation
8	Bang Pakong	13.50	100.98	tidal elevation
9	Bangkok Bar	13.43	100.58	tidal elevation
10	Chulachomklao Fort	13.57	100.57	tidal elevation
11	Mae Klong	13.38	100.00	tidal elevation
12	Pranburi	12.40	99.98	tidal elevation
13	Huahin	12.57	99.97	tidal elevation
14	Launsuan	9.93	99.10	tidal elevation
15	Ko Lak	11.80	99.82	tidal elevation
16	Ko Mattaphon	10.45	99.25	tidal elevation
17	Ko Prap	9.27	99.43	tidal elevation
18	Sichol	9.00	99.90	tidal elevation
19	Paknakorn	8.47	100.1	tidal elevation
20	Pakpanang	8.40	100.1	tidal elevation
21	Songkla	7.22	100.58	tidal elevation
22	Pattani	6.88	101.25	tidal elevation
23	Bang Nara	6.43	101.83	tidal elevation

Table D.1 Location of tide gauge stations

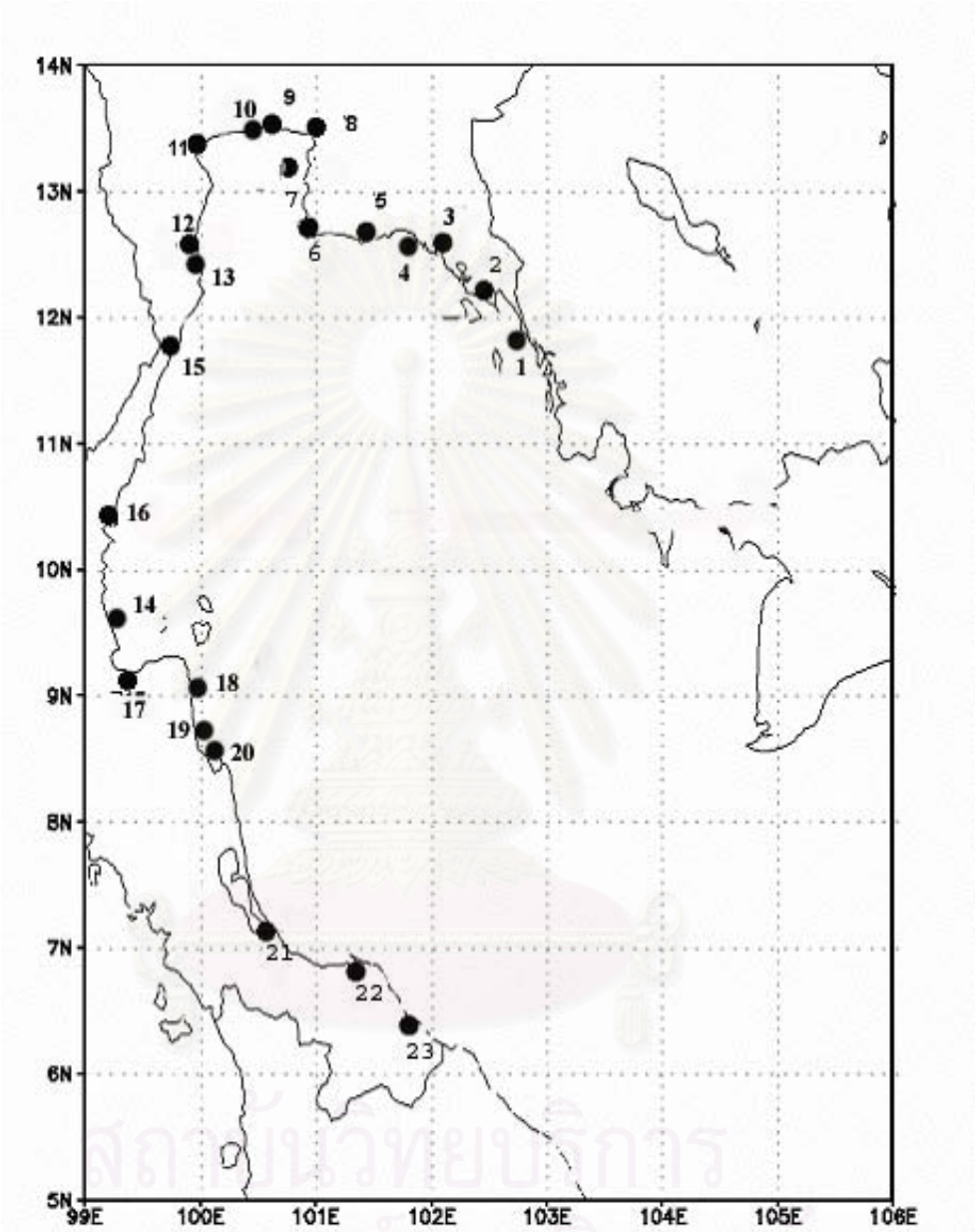

Figure D.1 Location of tide gauge stations (black circle)

APPENDIX E
TIDAL CONSTITUENTS

Tidal constituents	symbols	Angular speed (degree/hour)	Period(hour)
Semidiurnal components			
Declinational luni-solar	K_2	30.0821	11.97
Principal solar	S_2	30.0000	12.00
Principal lunar	M_2	28.9841	12.42
Larger elliptical lunar	N_2	28.4397	12.66
Diurnal components			
Declinational luni-solar	K_1	15.0411	23.93
Principal solar	P_1	14.9589	24.07
Principal lunar	O_1	13.9430	25.82
Larger elliptical lunar	Q_1	13.3986	26.87

APPENDIX F

THE BEST TRACK OF TYPHOON LINDA

On October 26, 1997, Typhoon Linda formed as the tropical disturbance within an area of convection east of the Philippine Islands near 10N 130E, and then moved westward under the subtropical ridge to the north. When entering the South China Sea, it transformed into a tropical storm and moved westward to the southern tip of Cape Camau of Vietnam at 0900Z on 2 November with the intensity of 55 kt (28 m/s). After that, it approached the Gulf of Thailand around 0030Z on 3 November with typhoon intensity and turned northwestward following steering from the subtropical ridge. Its strength weakened as it encountered mountains (Changwat Prachaubkirekhun). After crossing over the Andaman Sea, it reconsolidated and became typhoon once again at 0000Z on 6 November.

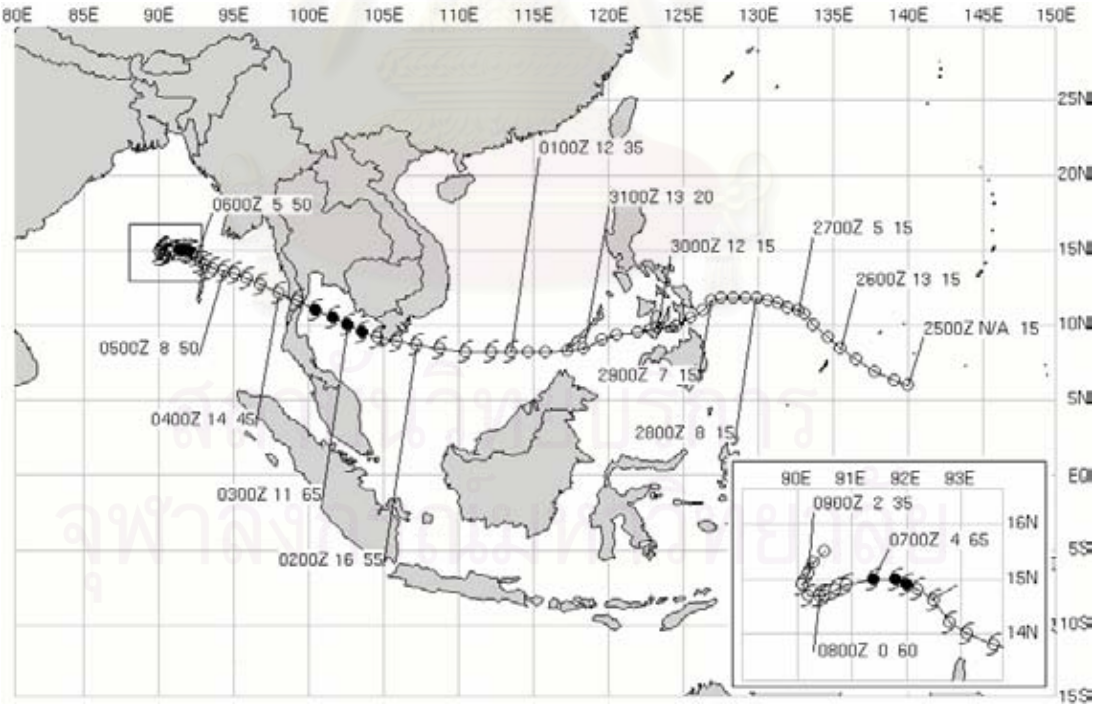

Figure F.1 The best track of Typhoon Linda

(**from**: https://metoc.npmoc.navy.mil/jtwc/atcr/1997atcr/ch3/30w.htm)

BIOGRAPHY

Jitraporn Phaksopa was born on 13 May 1980 in Yala. She received a Bachelor degree of Science in Physics from Prince of Songkhla University in 2000. In 2001, she entered a Master degree program at Department of Marine Science, Faculty of Science, Chulalongkorn University.